
Autogenous Shrinkage

Cementitious materials containing BFS

August 2011, Delft

Master Thesis

R.M. Mors

Thesis committee:

Prof.dr.ir. K. van Breugel	Materials & Environment
Prof.ir. A.Q.C. v.d. Horst	Structural & Building Eng.: Concrete Structures
Ir. W.J. Bouwmeester-van den Bos	Materials & Environment: Microlab
Dr.ir. E.A.B. Koenders	Materials & Environment: Modelling & Materials beh.
Dr.ir. E. Schlangen	Materials & Environment: Microlab
Ing. J. de Vries	Bouwdienst Rijkswaterstaat

Delft University of Technology
Faculty of Civil Engineering and Geosciences
Section Materials & Environment / Microlab

Preface

This report is the result of the work performed during the past eight months, in order to obtain the Master of Science degree in Civil Engineering at the Technical University of Delft. Research has been conducted for the Microlab at the section of Materials and Environment. Part of the laboratory experiments is executed there, the other part at the Stevin laboratories.

Many people assisted in establishing the thesis, therefore I would like to express my gratitude.

First I would like to thank the head of my graduation committee, Professor Klaas van Breugel. His interest in the topic, questions and guidance has been stimulating throughout the project.

Also thanks to the other committee members, for their view on the topic.

Especially my daily supervisor is greatly acknowledged, Jeanette Bouwmeester-van den Bos. Her enthusiasm, support and combined experience in practice and research have been of great help, both for the project aspects as for the research on concrete. For the part on cement paste Erik Schlangen has been of special help.

For execution of the experiments the people of the lab have been of great assistance, therefore thanks to: Edwin Scharp, Ton Blom, Fred Schilperoort, Arjan Thijssen en Ger Nagtegaal. For ideas regarding the Mini-TSTM, thanks go to Dongxing Xuan and Daniel Janssen.

In order to increase relevance, concrete mixtures used in this research are from practical cases. I am especially grateful to Ronald van Helden from Mebin to put mixture designs and resources at my disposal. Other thanks go to ENCI for providing cement.

Last but not least I would like to thank my family, friends, classmates and colleagues, their support, advice and good company have been very motivating.

Renée Mors
Alkmaar, June 2011

Abstract

In the Netherlands blast furnace slag cement is commonly used. Concretes with this type of cement are known for good durability properties. Where concrete is designed to crack in order to let the incorporated steel reinforcement take over tensile stresses, it is mainly for durability reasons that connectivity of cracks in concrete is undesired. Percolated cracks may lead to leakage problems or ingress of chemicals, which can cause deterioration of the concrete matrix or reinforcement corrosion.

When material deformations are restrained, stresses are induced, leading to possible cracking. Deformations in the early age are of most interest, with general properties of the concrete material still being developed. For the early age this is mainly caused by temperature and autogenous deformations, due to cement hydration.

Importance of autogenous shrinkage has been recognized for high performance concretes, having relatively low water to cement ratios. It is also becoming known that the magnitude of autogenous shrinkage is larger for materials containing blast furnace slag. As of late, even experiments on common normal strength concretes with higher water to cement ratios show a magnitude of autogenous shrinkage that can not be neglected.

This thesis gives an overview on the topic of autogenous shrinkage for normal strength concretes from practice, containing blast furnace slag. First to verify what has been found in previous research, furthermore to indicate practical relevance of the topic.

Main focus is on the influence of different material constituents, by changing the proportions or type of material. Magnitude of autogenous shrinkage is related to total shrinkage and compared to prediction models known in practice. Combined with results on general properties an indication is given for the possibility of cracking due to autogenous shrinkage.

Experiments on concrete regard influence of the water to cement ratio, aggregate type and addition of polypropylene fibres. Measurements start after one day and run for 197 days. Up to five specimens are used per test, which are either kept in autogenous conditions or are exposed to drying from 3, 7 or 28 days.

For experiments on cement paste a relatively new device is used, called the Mini-TSTM. Recommendations are given for ongoing development, but tests show promising results. It is possible to measure either free deformation or induced stress in case of restrained deformation. Cement pastes are used to determine influence of cement and filler type and content. Furthermore information is given on shrinkage development starting from the moment of initial set. Results on free deformation and self-induced stress under autogenous conditions are compared and show a reduced tensile strength when deformations are restrained.

Shrinkage development of blast furnace slag cement pastes seems substantially different from that of ordinary Portland cement paste, mainly steeper and of a higher magnitude. Changing aggregates from gravel to limestone reduces the shrinkage, but also the maximum strain by a similar value. Adding fibres to this mixture negates the shrinkage reducing effect, but a reducing effect on the maximum strain remains. Change of water to cement ratio seems to have negligible influence in this range of high water content. Also the filler material seems to have no influence for this particular proportion.

Results for tests on concrete show an ongoing shrinkage. From tests on cement pastes an expansion is found on the first 2~3 days. Combination of both results estimates the magnitude of tensile stress inducing shrinkage. Autogenous shrinkage is found to be half of the total shrinkage and is not to be neglected. At day 28 the magnitude of autogenous shrinkage approximates the elongation at break.

Measured total shrinkage relates well to the values from prediction models used in practice. In case of using blast furnace slag cement (CEM III/B) the subdivision into autogenous and drying shrinkage does quite differ.

The main recommendation is to not neglect autogenous shrinkage when blast furnace slag cement is used, even for normal strength concretes commonly used in practice.

Table of contents

Preface	i
Abstract	ii
Table of contents	iv
List of abbreviations	vii
1 Introduction	1
1.1 Scope of this thesis	2
1.2 Cement hydration	2
1.2.1 Clinker	3
1.2.2 Slag	4
1.3 Terminology	7
1.3.1 Autogenous shrinkage	7
1.3.2 Drying shrinkage	7
1.4 Mechanism shrinkage	8
1.4.1 Autogenous shrinkage	8
1.4.2 Drying shrinkage	11
1.4.3 Macroscopic expansion	13
1.4.4 Cracking	14
1.5 Influences of material	15
1.5.1 Mineral composition	16
1.5.2 Cement type	16
1.5.3 Water / cement ratio	17
1.5.4 Superplasticizer	17
1.5.5 Aggregates	17
1.5.6 Filler	17
1.5.7 Fibres	17
1.6 Reducing autogenous shrinkage	18
1.7 Objectives of this thesis	18
2 Methods	19
2.1 Materials	20
2.1.1 Mixture designs	20
2.1.2 Test programme	21
2.2 Testing procedures	22
2.2.1 Mixing and placing	22
2.2.2 Compressive and tensile splitting strength	23
2.2.3 Modulus of elasticity	23
2.2.4 Porosity	23
2.2.5 Autogenous and drying shrinkage concrete	23
2.2.6 Autogenous deformation and self-induced stresses in paste	24
2.3 Models	26
2.3.1 EuroCode	27
2.3.2 Japan Society of Civil Engineers (JSCE)	28

3	Results	31
3.1	Concrete general properties.....	32
3.1.1	Compressive strength	32
3.1.2	Maximum strain	33
3.2	Concrete shrinkage	34
3.2.1	Weight loss	34
3.2.2	Total shrinkage	35
3.2.3	Drying shrinkage and weight loss	37
3.2.4	Sealed shrinkage.....	39
3.2.5	Autogenous shrinkage	42
3.2.6	Comparison with prediction models EuroCode and JSCE.....	44
3.3	Cement paste	46
3.3.1	Free deformation	46
3.3.2	Self-induced stress.....	47
3.3.3	Maximum stress at restrained and free deformation	48
3.3.4	Porosity.....	49
3.4	Combination concrete and cement paste	50
4	Discussion	51
4.1	Discussion results	52
4.2	Limitations of Mini-TSTM	54
4.3	Conclusions	56
4.4	Recommendations	57
4.4.1	Practice, EuroCode.....	57
4.4.2	Development Mini-TSTM.....	57
4.5	Future research	58
	References	60
	Appendices	65
	Appendix A Particle size distribution materials pastes	
	Appendix B Total shrinkage concrete until 196 days	

List of abbreviations

A	Al ₂ O ₃ , Aluminium Oxide
ACI	American Concrete Institute
ADTM	Autogenous Deformation Testing Machine
AFm	Here: Monosulphate, from Al ₂ O ₃ -Fe ₂ O ₃ -mono
AFt	Here: Ettringite, from Al ₂ O ₃ -Fe ₂ O ₃ -tri
ASTM	American Society for Testing and Materials
BFS	Blast Furnace Slag
C	CaO, Calcium Oxide
C/S	Ratio of CaO to SiO ₂
C ₂ S	Dicalcium Silicate, Belite
C ₃ A	Tricalcium Aluminate
C ₃ S	Tricalcium Silicate, Alite
C ₄ AF	Tetracalcium Aluminoferrite
CH	Calcium Hydroxide, Portlandite
CSH	Calcium Silicate Hydrate
CTE	Coefficient of Thermal Expansion
EC	EuroCode
EN	European Norm
ESEM	Environmental Scanning Electron Microscope
HPC	High Performance Concrete
HT	Hydrotalcite
JCI	Japan Concrete Institute
JSCE	Japan Society of Civil Engineers
LSP	Limestone Powder
LVDT	Linear Variable Differential Transformer
LWA	Lightweight Aggregate
M	MgO, Magnesium Oxide
MIP	Mercury Intrusion Porosimeter
MSA	Mineral Shrinkage-compensating Admixture
NBN	Belgisch bureau voor Normalisatie
NEN	Nederlandse Norm
NIST	National Institute of Standards and Technologies
OPC	Ordinary Portland cement
PP	Polypropylene
PSD	Particle Size Distribution
RH	Relative Humidity
RILEM	Réunion Internationale des Laboratoires d'Essais et de recherche sur les Matériaux et les Constructions
ROBK	Richtlijnen voor het Ontwerpen van Betonnen Kunstwerken
S	SiO ₂ , Silicate
\bar{S}	SO ₃ , Sulphur Trioxide
SAP	Super Absorbent Polymers
SPL	Superplasticizer
SRA	Shrinkage Reducing Admixture
TSTM	Temperature Stress Testing Machine
w/c, wcr	Water to Cement Ratio

Chapter 1

Introduction

First the scope of the thesis is identified, followed by a literature review. A short description of cement hydration is included, together with definitions, mechanisms and other relevant issues concerning the phenomenon of autogenous shrinkage. The chapter concludes with the aim and objectives of the thesis.

1.1 Scope of this thesis

Together with Japan, the Netherlands is a major player in the use of blended cements containing blast furnace slag (BFS). Slag is a by-product of the steel industry and therefore considered a sustainable alternative to ordinary Portland cement (OPC). Concrete with slag cement is known for good durability properties, due to the dense microstructure and low alkali levels in the pore water. Where concrete is designed to crack in order to let the incorporated steel reinforcement take over tensile stresses, it is mainly for durability reasons that non structural cracking in concrete is undesired and a lot of attention is paid to this issue. Percolated cracks may lead to leakage problems or ingress of chemicals, which can cause deterioration of the concrete matrix or reinforcement corrosion.

When deformations of the material are restrained, stresses may occur that can lead to crack formation. Deformations in the early age are of most interest, with general properties of the concrete material still being developed. For the early age this is mainly caused by temperature and autogenous deformations, due to cement hydration.

Sensitivity for early-age cracking is commonly known for high-performance concretes (HPC) with a low water to cement ratio, where the phenomenon of autogenous deformation is of recognized importance. As of late striking results have been found regarding the magnitude of autogenous shrinkage for normal strength concretes commonly used in the Netherlands, using slag cements and relatively high water cement ratio (van Cappellen, 2009). A clear explanation cannot be given. In practical cases increasing early age cracking is witnessed for comparable mixtures. Since temperature and curing are controlled during the execution, the cause needs to be found elsewhere. Using such a complex material it is probable that a combination of factors has lead to the eventual cracking. This research will focus on the possibility of autogenous shrinkage as one of the causes.

Main ideas on autogenous shrinkage are based on the use of ordinary Portland cement (OPC), but it has already become apparent that mineral admixtures change the behaviour significantly. Influence of fineness of the binder material has also been determined. Focus of this thesis does not lie on the binder material, but on the different constituents in a concrete mixture.

Basis in the research is conventional concrete and is compared to a more recent application in the building industry, namely fire resisting concrete. Information is used from a practical case in the Netherlands. Instead of gravel, limestone is used as a coarse aggregate, with a thermal expansion coefficient close to that of cement paste. Polypropylene (PP) fibres are mixed in, under high temperature the fibres evaporate, leaving space for the internal moisture transport, relieving upbuilt of pressure. Superplasticizer is used for workability of the mixture. An additional limestone filler is used to stabilize the mixture (van den Bossche, 2008).

1.2 Cement hydration

Hydration of cement is a complex interaction between water and the material compounds, which are mainly the minerals C_3S , C_2S , C_3A and C_4AF . Through chemical reactions hydration products are formed, creating a “stone-like” material. The process is ongoing in time. Cement used in this research regards a blend of Portland cement clinker and blast furnace slag. Blast furnace slag acts like a pozzolanic material. There is more complexity to the hydration of blended slag cements, because hydration of both constituents occurs simultaneously and interferes with each other. An overview is given of microstructure formation at hydration of clinker and pozzolanic reaction of slag.

1.2.1 Clinker

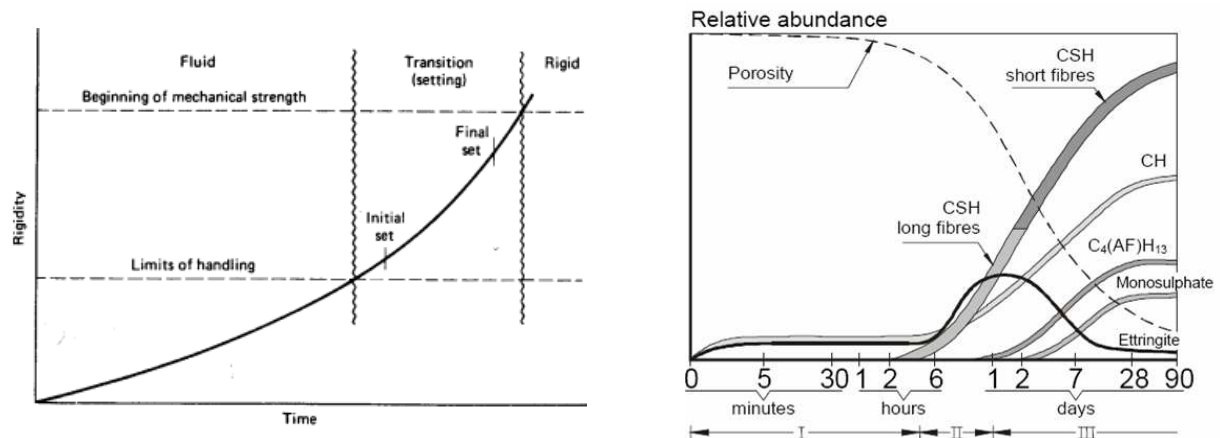


Figure 1 Left: Rigidity phases, liquid, hardening transition and rigid (Mehta & Monteiro, 1993)
Right: Three phases in formation hydration products of Portland cement (Locher et al., 1976)

Three phases in the rigidity of hydrating cement paste can be recognized (Figure 1), induced by several stages in the hydration of Portland cement clinker (Figure 2).

First is the liquid phase. Rapid reaction takes place when cements grains come in contact with water. This initial hydrolysis (stage I) causes reaction of C_3A with gypsum and water to form ettringite and lasts only a few minutes, followed by the nucleation controlled dormant period (stage II), characterized by several hours of continued dissolution of ions with little hydration. Second phase is transition. First is chemical controlled acceleration (stage III), with initial formation of hydration products. C_3S and C_2S are the principal components of Portland cement and react with water to form amorphous CSH and crystalline CH. Furthermore aluminates C_3A and C_4AF continue to hydrate and form ettringite (AFt phase), subsequently converted to the more stable monosulphate (AFm phase). Formation of outer products leads to interconnection of cement particles, forming a solid skeleton. The mineral percolation threshold occurs when the first solid linear path has been created in the cementitious system (Bentur, 2002). For pastes the Vicat test is used to determine the upper and lower bound for this time, giving initial and final set. Acceleration is followed by deceleration (stage IV), which is chemical and diffusion controlled. At a slower rate formation of hydration products continues, which gives the rate of early strength gain. The suspension-solid transition occurs when percolation of the network appears in three dimensions.

Last is the rigid phase. The rate of later strength gain by formation of hydration products is at steady state (stage V) and is controlled by ions diffusing through the layer of hydrates.

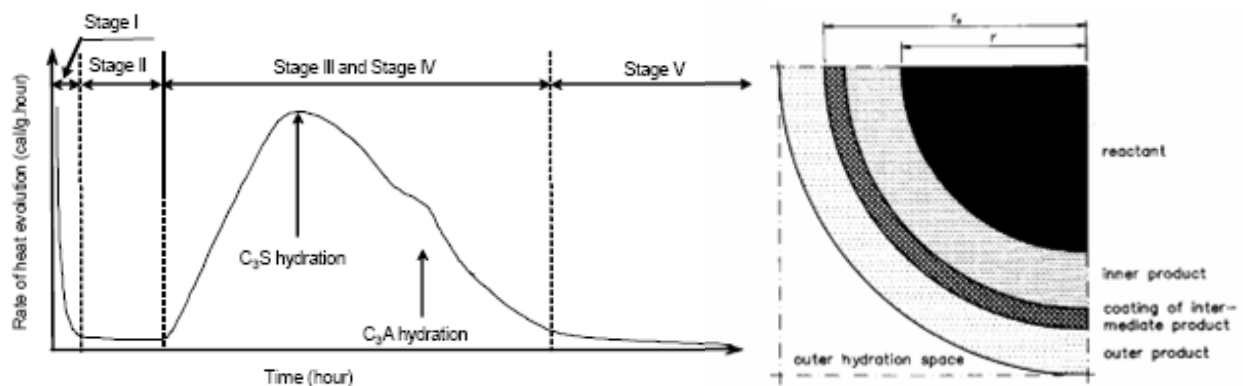


Figure 2 Left: Hydration stages of Portland cement (after Mindess and Young, 1981)
Right: Conceptual view of hydrating C_3S particle (after Kondo et al., 1968)

1.2.2 Slag

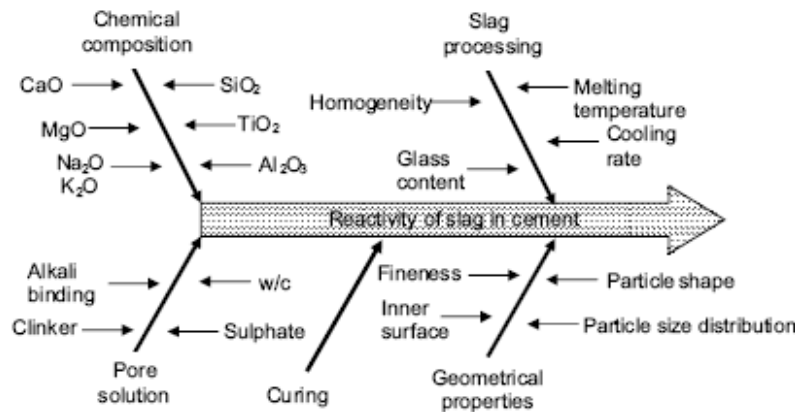


Figure 3 Factors on the reactivity of slag (after Wolter et al., 2003)

Blast furnace slag is a latent hydraulic material, meaning that in order to trigger the reaction an activator is needed to be present. In blended cements the Portland cement is used as activator, combining the effect of alkali hydroxides, gypsum and CH.

Among others, reactivity of slag is dependent on particle shape and size (Figure 3). Where the thickness of the hydrated layer of a slag particle is not dependent of the particle size, fine slag particles are expected to hydrate much faster than coarse ones, there the rate of hydration is related to the surface area (Sato et al., 1986).

Figure 4 gives an conceptual view of hydration products at a slag particle, where the rate of hydration of slag is comparable to that of C_2S in Portland cement (Taylor, 1997). Tanaka & Totani [1983] conducted experiments with SEM to show hydration of slag. First the slag particle is covered by Portland cement hydration products, then an inner hydrated layer is produced due to reaction with Ca^{2+} ions from the supersaturated solution. Subsequently a skeleton of hydrated layers is left from dissolution of Ca^{2+} and Al^{3+} ions from the slag particle.

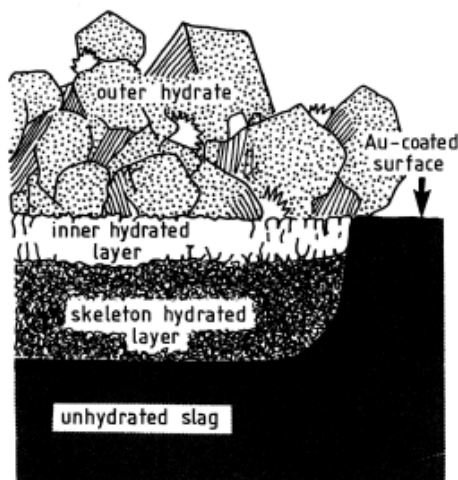


Figure 4 Slag hydration products in hydrating blended cement paste (after Tanaka & Totani, 1983)

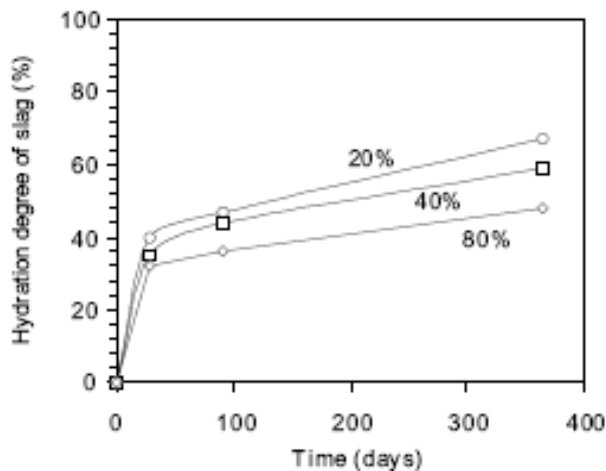


Figure 5 Hydration degree of slag in blended cement paste with different slag proportions, $w/c=0.5$, $T=20^{\circ}\text{C}$ (after Schäfer, 2004)

Chen [2006] built a reaction model for the slag-blended cement, based on stoichiometry using oxide compositions of the initial materials. The model showed a good fit with experimental data and is also coherent with previous results (Pietersen, 1993). In the model part of the CH from the clinker hydration enters the CSH produced from the slag reaction, where the amount is related to the blend proportions. Even though the C/S ratio in CSH is lower in slag cement than in Portland cement, it is still higher than the C/S ratio of anhydrous slag, which means this external Ca^{2+} source is needed.

Hydration degree of slag remains low. For w/c lower than approximately 0.40, pastes densification impedes hydration of slag due limited space in capillary pores for the growth of hydration products. For higher w/c hydration degrees of slag do not vary significantly. Hydration is governed by dissolution, depending on slag reactivity, pore water composition and contact with water. The increment of degree in time remains existent (Figure 5), therefore long-term properties may keep changing significantly at later ages. Lower hydration degrees result from higher slag proportions in the cement.

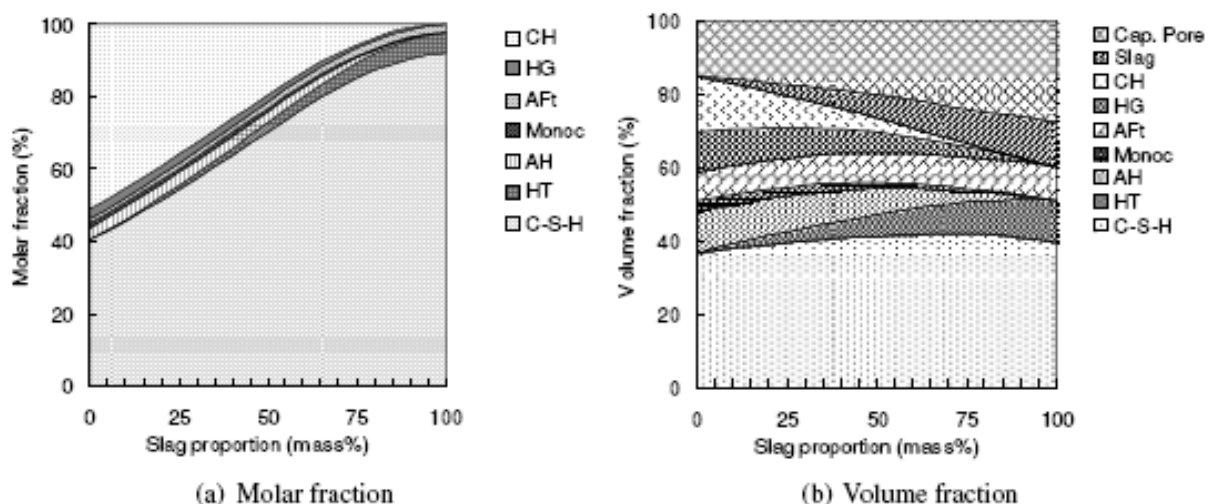


Figure 6 Molar fractions of hydration products and volume fraction of phases in hydrating slag-blended cement paste, $w/c=0.5$, $\alpha_{\text{cement}}=100\%$, $\alpha_{\text{slag}}=70\%$ (Chen, 2006)

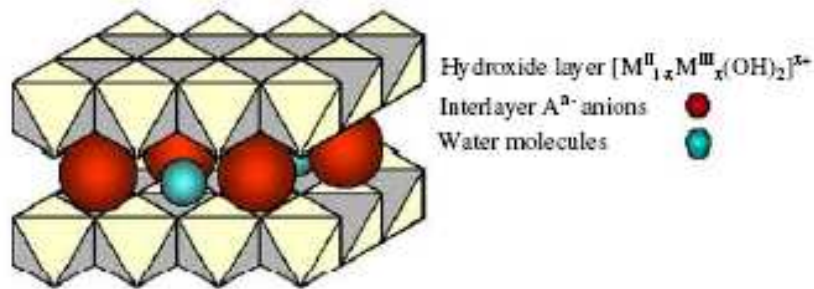


Figure 7 Layered structure of hydrotalcite-like compounds (Chen, 2006)

Figure 6 shows hydration products with increasing slag proportion. First the slag content A is combined with M and forms hydrotalcite, combined with \bar{S} ettringite is formed. Remaining A substitutes for S in CSH, when the maximum substitution is reached remaining A reacts to an AFm phase. Other than a reduction of CH and increased proportions and morphological change of CSH by slag hydration, an additional hydrate is formed, hydrotalcite (HT).

Compared to Portland cement paste, pore solution of slag cement paste contains a remarkable amount of sulphide, so that AFt may remain stable. Alkali concentrations in the pore solution are depressed, as also found in other research (Lura, 2003). Though CSH in slag cement paste may have some alkali binding capacity, the main binding property is given to the hydrotalcite. Hydrotalcite has a layered crystalline structure, with a large specific area and high anion-exchange and cation binding capacities (Figure 7).

1.3 Terminology

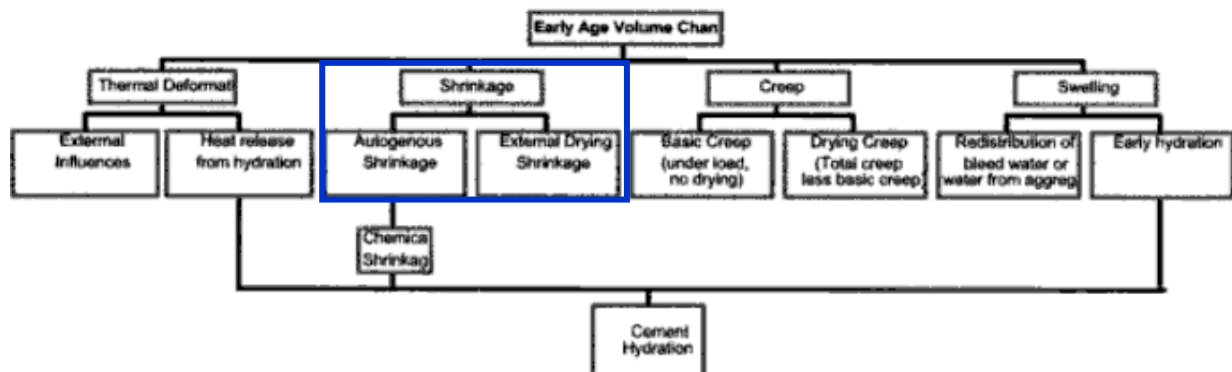


Figure 8 A phenomenological summary of (early age) volume change (Lange, 2002)

Volume change of cementitious systems has several causes, among which one regards shrinkage (Figure 8). Total shrinkage consists of autogenous and drying shrinkage. For both the definition is given.

1.3.1 Autogenous shrinkage

Terminology regarding the phenomenon of autogenous deformation is opted from the Autoshrink'98 Workshop by JCI (Tazawa, 1998). Autogenous deformation is caused by cement hydration and seen as the external, macroscopic volume change of cementitious materials after initial set, without any “exchange” with the environment. This exchange is either of substances (moisture), a temperature variation or an external load or restraint. Volume change is either a volume reduction, shrinkage or a volume increase, expansion. Autogenous deformation is essentially volumetric, three dimensional. Within the framework of this investigation the one dimensional, linear length change is regarded, called strain.

1.3.2 Drying shrinkage

Drying shrinkage is the time-dependant volume reduction due to loss of water at constant temperature and relative humidity (Hansen, 1987).

1.4 Mechanism shrinkage

Autogenous and drying shrinkage are in a way related, mechanisms behind these phenomena will be explained. In the saturated state at early age expansion may occur, this may positively contribute by counteracting the shrinkage and therefore prolonging the time until harmful shrinkage. The way in which the deformations may lead to cracking will also be shown.

1.4.1 Autogenous shrinkage

The phenomenon of autogenous shrinkage can be explained by theories on cement hydration. The mechanism of autogenous shrinkage concerns the volume change of the hydrating cement paste and the therewith induced internal drying on the longer term. How autogenous shrinkage relates to the hydration is explained next.

Le Chatelier [1900] was first to determine a significant reduction of the absolute volume of a cementitious material during cement hydration. From stoichiometry following the hydration kinetics it is shown that the original volume of reacting constituents (water and cement) is higher than the absolute volume of the hydrates formed in the reaction. This creation of voids is the internal-microscopic volume change, named chemical shrinkage. In a RILEM report, Barcelo [2002] gives a graphical representation of the volumetric balance of hydration, as included in Neville [1995]. Also on the macroscopic scale a volumetric change can be witnessed, after initial set this is the phenomenon of autogenous shrinkage (Figure 9).

Figure 10 distinguishes the different stages in rigidity of the hydrating cementitious material, affecting the ratio between external and chemical shrinkage (Acker, 1988). In the liquid phase (AB) the external shrinkage is equal to the internal shrinkage which is purely caused by the chemical changes, because the material has no resistance to the volume change. From initial set, onset of formation of a skeleton, this chemical shrinkage gets more and more restrained (BC). After final set (beyond point C), the material becomes rigid. After formation of a rigid skeleton the volume change of hydration leads to increasing internal porosity, but hardly to external shrinkage. External volume change becomes governed by another consequence of the cement hydration, namely the water consumption.

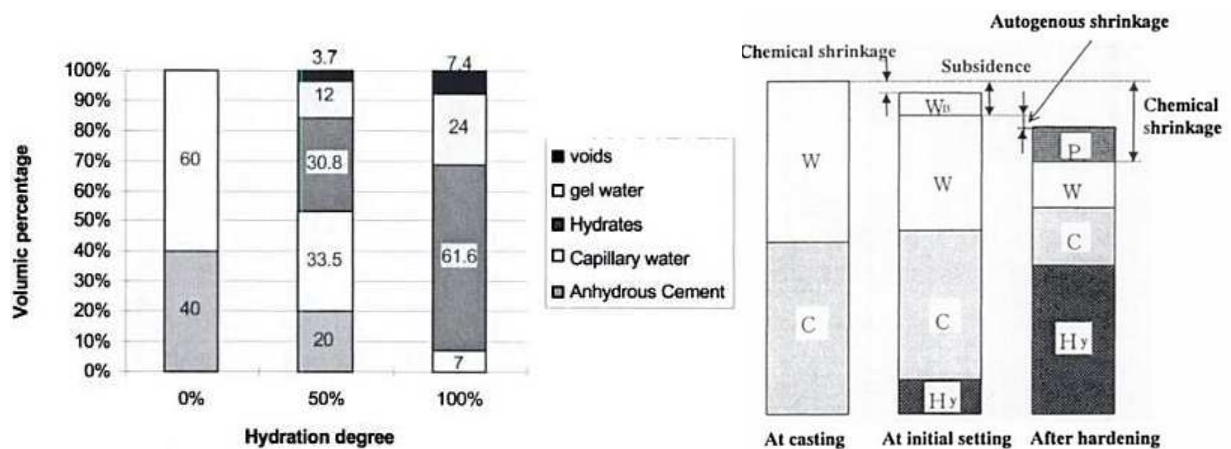


Figure 9 Left: Volumetric balance of hydration (according to Neville, 1995)
 Right: Autogenous and chemical shrinkage (Tazawa, 1998), where:
 C = unhydrated cement, W = unhydrated water, P = voids generated by hydration,
 H_y = hydration products, W_b = bleeding water

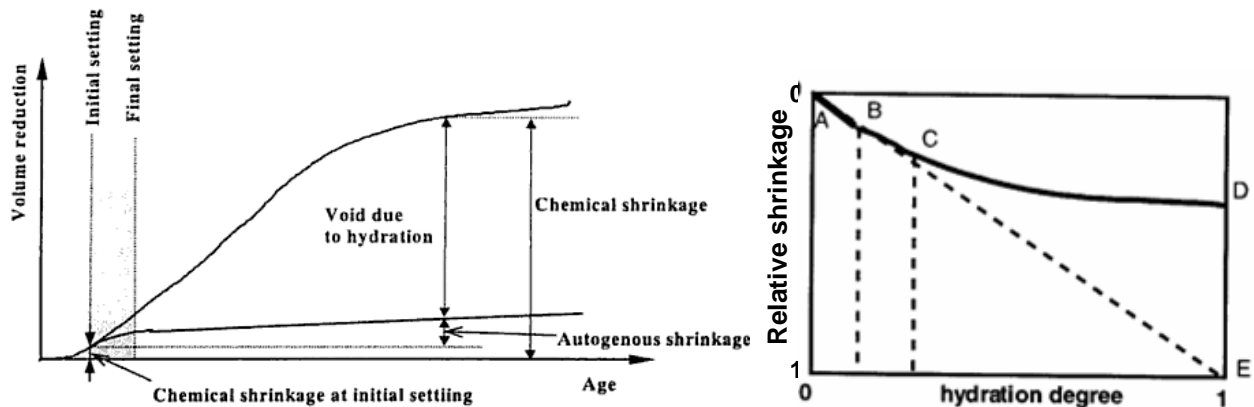


Figure 10 Left: Relation between chemical shrinkage and autogenous shrinkage (Tazawa, 1998)
 Right: Schematic evolution relative shrinkage as a function of hydration degree (Acker, 1988),
 with relative shrinkage = external shrinkage / chemical shrinkage

Observed external shrinkage is ascribed to the physical phenomenon of arising capillary action in the pore water, known in soil mechanics as suction forces. This is caused by the continuous consumption of water by the cement hydration. Reduction of pore volume proceeds at a slower rate than the reduction of the water volume, so that pores will be partially emptied. The decrease in internal relative humidity is known as “self-desiccation”. This even takes place in a saturated state due to the depercolation of pores (Geiker & Knudsen, 1982). Figure 11 shows the retreat of capillary water to the smaller pores, which happens for thermodynamic reasons (Lura, 2003). As a consequence of the occurring capillary suction forces, the surrounding matrix of hydration products becomes compressed and wants to reduce in volume. Depending on the compressibility of the material shrinkage occurs. Because concrete for the larger part consists of aggregates, magnitude of the externally observed shrinkage of concrete is mainly influenced by the rigidity of aggregates, which act like internal restraints. A substantial reduction is found on the magnitude of shrinkage when compared to pastes, 30 to 45% according to literature (Iragashi et al., 1999). Increasing stiffness of aggregates leads to a decrease in shrinkage.

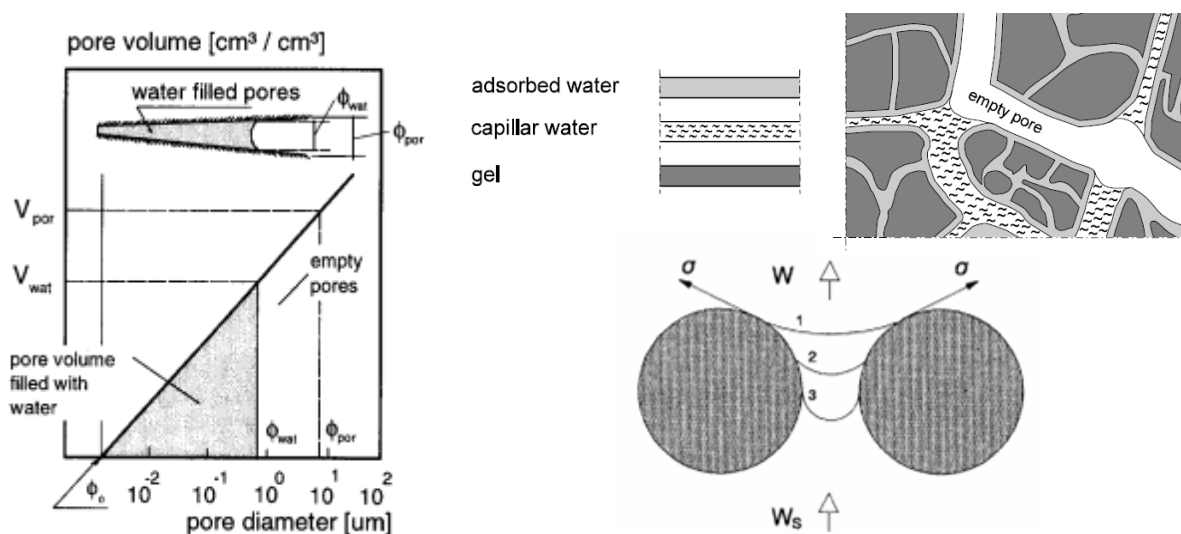


Figure 11 Left, right upper: Schematic representation of the pore size distribution with emphasis on the state of the pore water within the total pore volume (van Breugel, 1991)
 Right lower: Stresses pulling the water meniscus lower between two cement particles due to moisture transfer and capillary pressure development (Radocea, 1992)

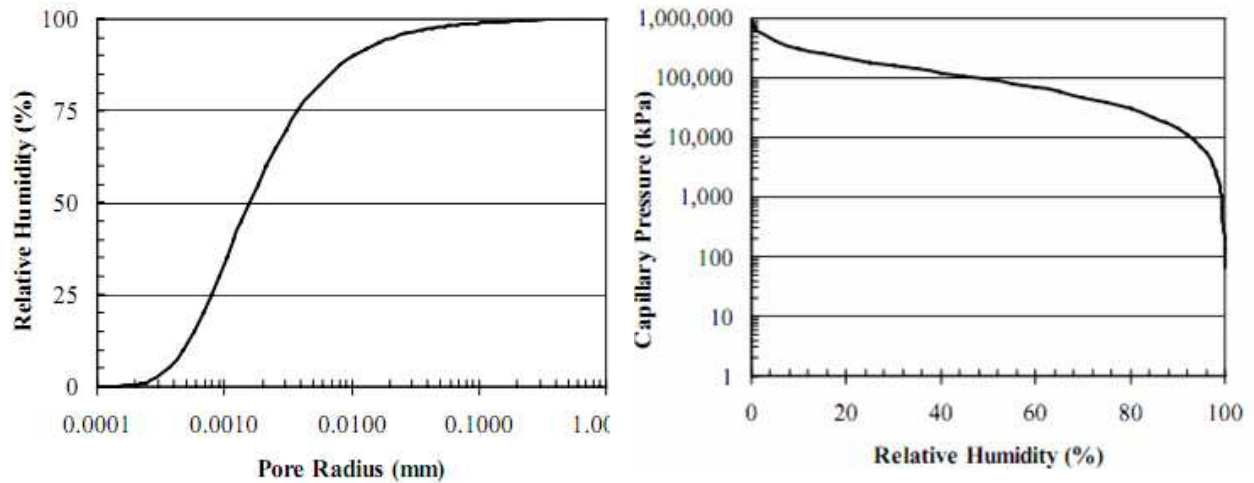


Figure 12 Left: Relation RH and empty pore radius, based on Kelvin's equation (Holt, 2001)
Right: Relation RH and suction, based on Laplace and Kelvin equations (Holt, 2001)

Capillary forces or suction are a function of radius of curvature of the meniscus between water and air, as given by the equation of Laplace:

$$\sigma_{cap} = -\frac{2\gamma}{r} \quad (1.1)$$

The difference in surface tension of the pore fluid, γ , is negligible for the used materials (Lura, 2003), so that a reduction of pore radius, r , leads to an increase in capillary stress, σ_{cap} .

Kelvin gives the RH drop due to menisci formation and can be combined with Laplace:

$$RH = \exp\left(-\frac{2\gamma M}{r\rho RT}\right) \xrightarrow{Laplace} RH = \exp\left(-\frac{\sigma_{cap} M}{\rho RT}\right) \quad (1.2)$$

An increase in capillary stress leads, together with a number of constants (molecular weight M and density ρ of water, gas constant R and temperature T), to a decrease in relative humidity, RH . Figure 12 shows both in graphic form.

Deformation of cement paste is given by the following equation (Bentz et al., 1998):

$$\varepsilon_{LIN} = \frac{S \cdot \sigma_{cap}}{3} \cdot \left(\frac{1}{K_P} - \frac{1}{K_S}\right) \quad (1.3)$$

The linear strain, ε_{LIN} , is mainly dependent on the saturation fraction, S , and the capillary tension. A change in bulk modulus of the whole porous body, K_P , and bulk modulus of the solid material, K_S , may lead to a 6% difference (Lura, 2003). The saturation fraction is the ratio of evaporable water content, V_{ew} , and the total pore volume, V_P , which both depend on the w/c and the degree of hydration.

Figure 13 shows that the internal relative humidity of BFS cement pastes is lower after a certain time than that of OPC paste (Lura, 2003). Therefore higher capillary pressure can be expected and thus enhanced shrinkage in case of BFS cement.

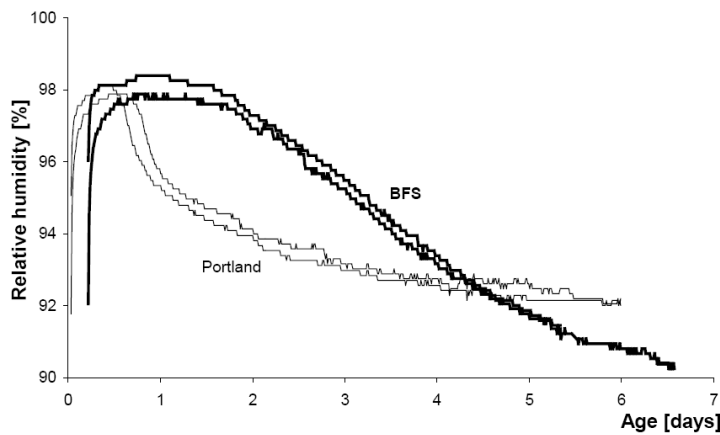


Figure 13 Internal RH versus age for OPC and BFS cement paste (Lura, 2003)

Another mechanism regards adsorbed water in the pores. For the deformation mechanism, Bangham [1937] was first to propose an equation that relates swelling to changes in surface tension. He did this for coal and later also validity was shown for cement paste upon wetting (Wittmann, 1977). Koenders [1997] used the same relationship for autogenous deformation:

$$\frac{\Delta l}{l} = \lambda \cdot \Delta \gamma \quad (1.4)$$

The ratio of change of length, Δl , and length, l , relates to the change in surface tension of the solid particles, $\Delta \gamma$, by a proportionality coefficient, λ . The surface tension in the surface layer will increase with decreasing RH in the pore system, with highest influence below 40% RH.

$$\lambda = \frac{\Sigma \cdot \rho_{sol}}{3 \cdot E} \xrightarrow{\text{Koenders}} \lambda(\alpha, RH, wcr) = \frac{[A_{pore}(\alpha) - A_{wat}(\alpha, RH)] \cdot \rho_{paste}(wcr)}{3 \cdot E_{paste}(\alpha)} \quad (1.5)$$

Proportionality of the microstructural deformations is dependent on the paste density, ρ_{paste} , and paste stiffness, E_{paste} . Since water is considered incompressible, the mechanism of surface tension for volumetric changes acts on the solids alone (Powers, 1965). Therefore the pore wall area per unit weight, Σ , is changed to the pore wall area of the empty pores, $A_{pore} - A_{wat}$. Now the proportionality becomes dependent on the RH, which makes the model also suitable for a RH higher than 40%, where disjoining pressure is considered the cause (Figure 14).

Figure 15 shows for later ages a linear relation between change in internal relative humidity and free autogenous shrinkage (Baroghel-Bouny, 1996). With an approximately constant stiffness, the length change becomes purely dependent on the relative humidity and can therefore be expected to be linear.

1.4.2 Drying shrinkage

Mechanisms of autogenous and drying shrinkage are similar, both related to internal RH drop. In case of autogenous shrinkage RH decrease is due to hydration, for drying shrinkage this is caused by moisture exchange with the environment. Transport is driven by pressure gradients between the “water-rich” capillary system and “water-poor” surrounding atmosphere, where movement reduces in less permeable microstructures. Evaporation is concentrated at the exposed surfaces and drying shrinkage is therefore not uniform throughout the cross-section.

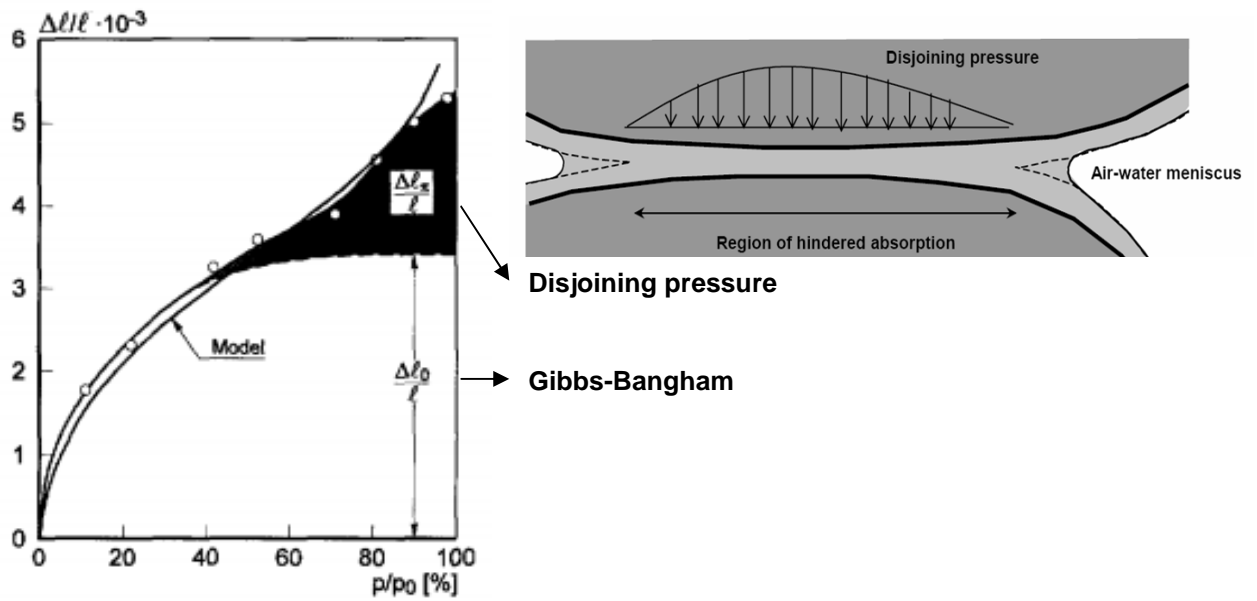


Figure 14 Left: Swelling of hardened cement paste versus RH combined with model (Koenders, 1997)
 Right: Disjoining pressure at surfaces of hindered adsorption (after Soroka, 1979)

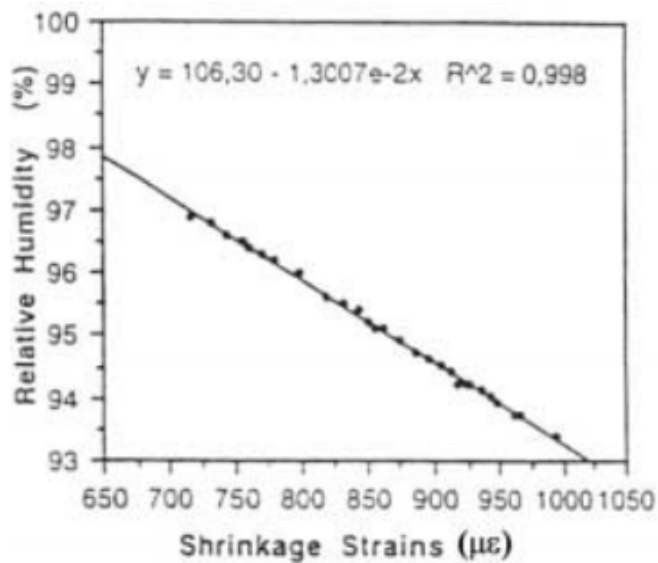


Figure 15 Correlation between free autogenous shrinkage strains and internal RH of the materials, measured at $T = 21^\circ\text{C}$, from 28 days (Baroghel-Bouny, 1996)

1.4.3 Macroscopic expansion

Le Chatelier [1900] observed expansion for hydrating cement pastes in saturated conditions. It is expected in high w/c cement pastes, since these pore systems are supposed to remain saturated throughout hydration (Neville, 1995).

Bjøntegaard [1999] sees reabsorption of bleeding water as the principal cause of swelling at early ages. According to Lura [2003] bleeding water reabsorption itself cannot be the reason of expansion, until all water is sucked into the paste or removed, the system remains saturated and therefore no internal RH change occurs.

In saturated state expansion may show because expansion of solid phases is not opposed by capillary pressure upbuilt (Powers, 1935). Even in the early stage reaction products form a spatial network, due to their shape. Internal pressure is caused by further growth of hydrates inside the network, causing moderate swelling of the system (Bažant & Wittmann, 1982). Given the large surface area of reaction products, disjoining pressure acts on a growing area producing expansion (Wittmann, 1992).

Pressure from solid phase growth can for instance apply to formation of CH crystals or ettringite. For the latter Jensen [1993] calculated a value of about 16 MPa, high enough to create relevant expansion. For shrinkage reduction care should be taken since expansion due to crystallisation can be a localized phenomenon, where chemical and autogenous shrinkage are fairly uniform throughout the cementitious system (Chen, 2006). If ettringite formation takes place in the fluid state, expansion does not contribute to any pressure development. Given the high water consumption of ettringite, it is more likely to cause additional shrinkage at a later stage when converted to monosulphate. With the length over thickness ratio of ettringite dependent on the pH (Figure 16), relatively longer needles are expected in BFS cement paste compared to OPC paste, given the lower alkali content of the pore solution.

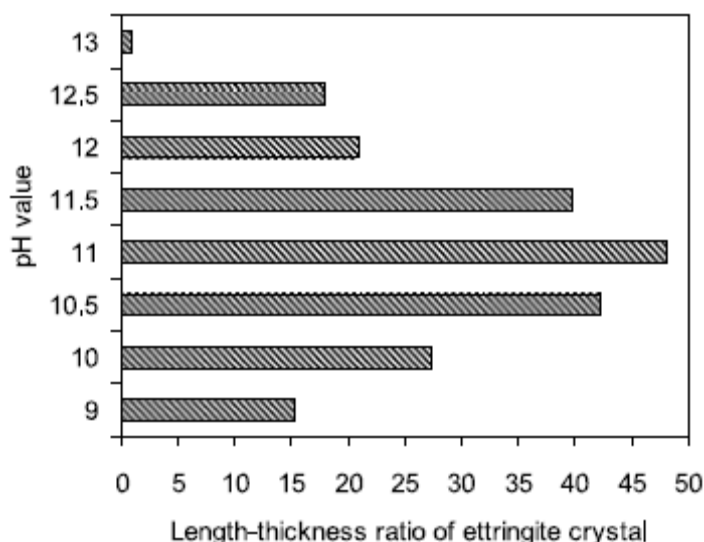


Figure 16 Effect pH solution on length/thickness of ettringite crystals (after Chartschenko & Stark, 1995)

1.4.4 Cracking

Figure 17 shows subsequent stages for deformation induced stress. After casting the concrete the mixture is still fluid and cannot sustain any loads. Deformations can occur without hindrance. From the moment a supporting structure is formed, hindrance of deformations may cause stresses. Restraint can be by other structural elements against which the new element is cast. Internal restraints may be caused by aggregates or steel reinforcement leading to internal cracking. Restrained expansion puts the material in compression, which does not need to cause problems. Restrained shrinkage leads to tensile stresses, when the occurring stresses are larger than the ultimate tensile strength, the material cracks (Figure 18).

Calculation of restraint can be done by the following equation (Bentur, 2002):

$$\% \text{ restraint} = [K_r / (K_s + K_r)] \cdot 100 \quad (1.6)$$

Ratio of the stiffness of the restraining member, K_r , and the shrinkage element, K_s , gives the degree of restraint. For early age concrete in a typical bridge element, including reinforcing steel bars this was calculated to be up till 98%, because of the low modulus of elasticity. For matured concrete in this typical element calculation came to a restraint of about 33%.

Multiplication of shrinkage strain and modulus of elasticity according to Hooke does not give the actual tensile stress. Internal redistributions lead to relaxation of the material, so that under sustained deformation a reduction in stress occurs (Figure 19).

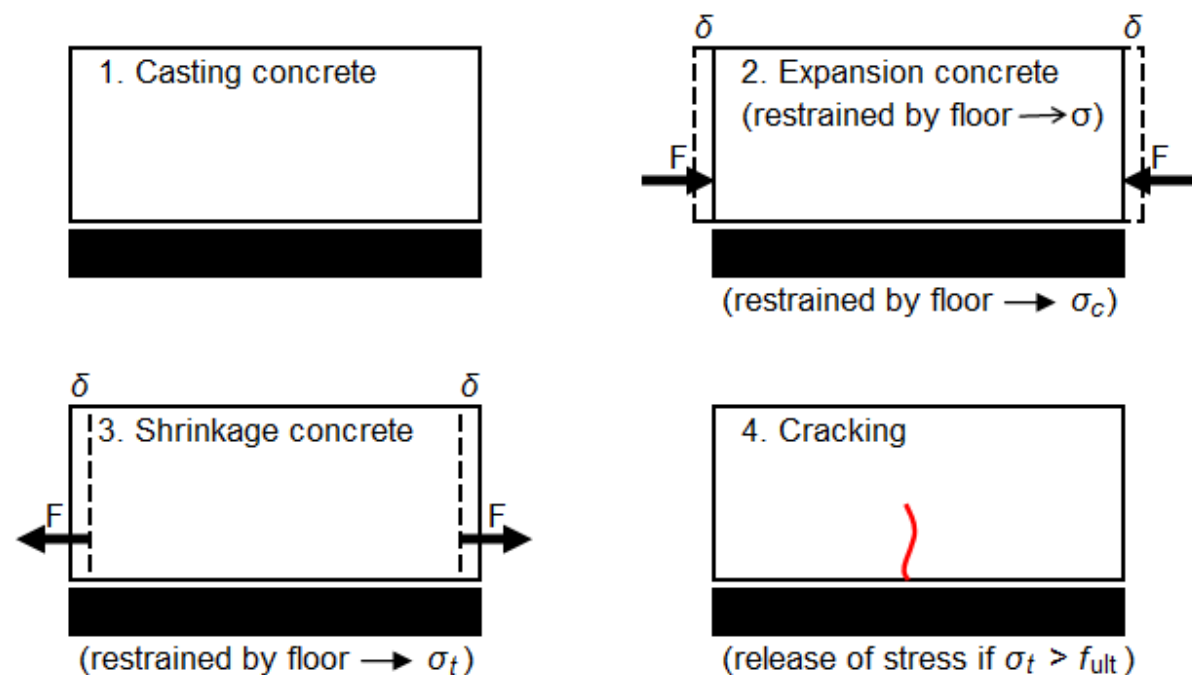


Figure 17 Mechanism of shrinkage induced cracking

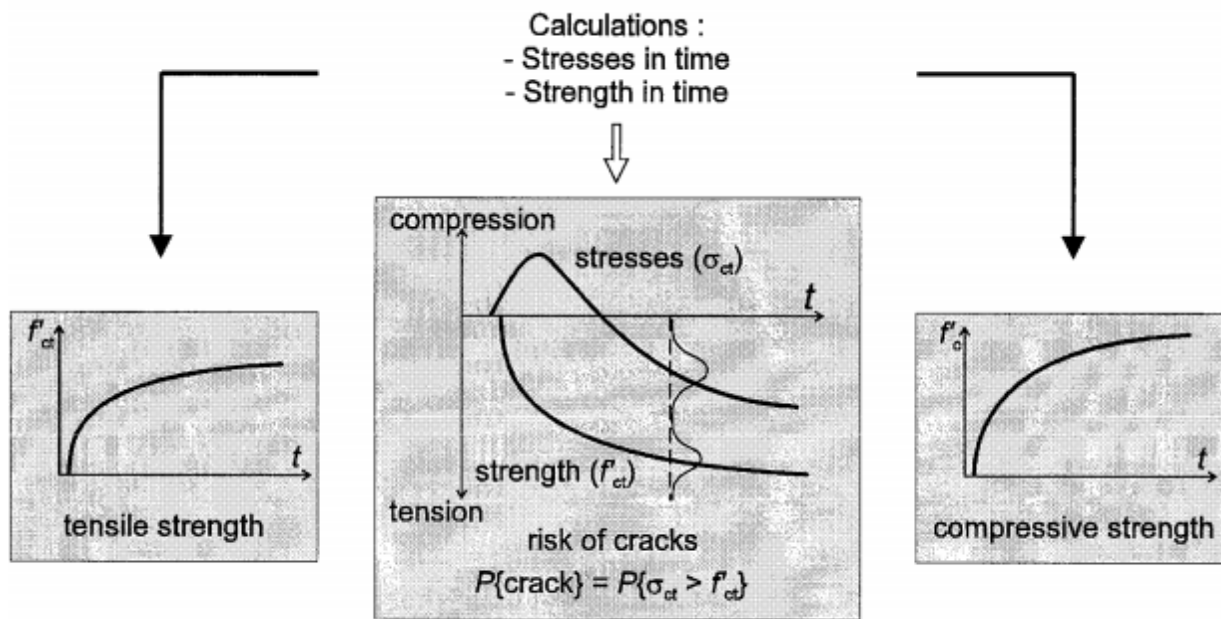


Figure 18 Schematic representation for qualification concrete cracking (van Beek, 1995)

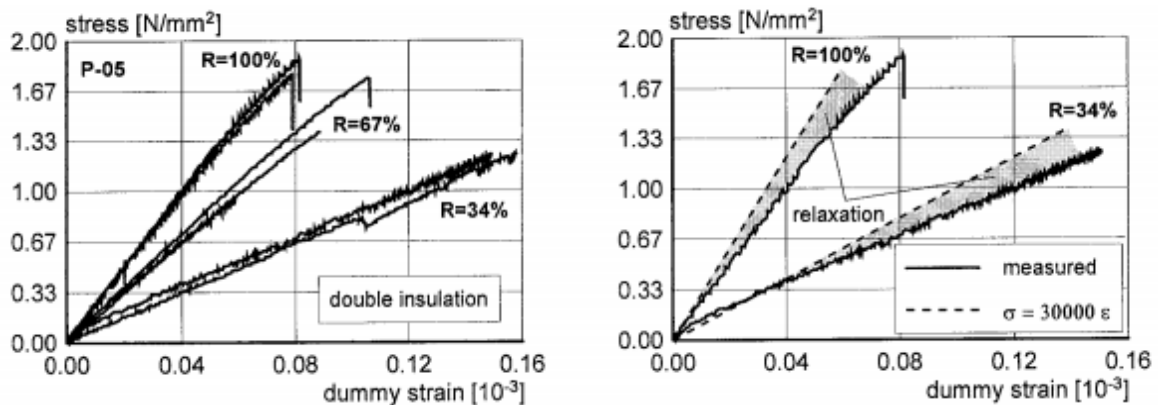


Figure 19 Left: development tensile stress at various restraints as function of unrestrained deformations. Right: measured stresses compared to calculated elastic stresses (Lokhorst, 1999)

1.5 Influences of material

According to Holt [2001] autogenous shrinkage cannot be controlled by construction practice, only the mixture design can have an influence. Early age autogenous shrinkage can be of the same order of magnitude as shrinkage on the long term and should be taken into account. During the very first hours autogenous shrinkage is closely related to chemical shrinkage, thus cement chemistry and fineness have a great influence. A delay in the stiffening and strength development of concrete will lengthen the period of early age autogenous shrinkage and can be caused by mixture parameters. Shrinkage is higher when superplasticizer is added, due to better cement dispersion. Shrinkage may be higher if the setting time is delayed, which can for instance be caused by chemical admixtures or temperature.

1.5.1 Mineral composition

Research has shown strong dependence of autogenous shrinkage on mineral composition of cement (Miyazawa & Tazawa, 2005). The proposed prediction model is based on Bogue:

$$\varepsilon_p(t) = A \cdot \alpha_{C_3S}(t) \cdot (C_3S\%) + B \cdot \alpha_{C_2S}(t) \cdot (C_2S\%) + C \cdot \alpha_{C_3A}(t) \cdot (C_3A\%) + D \cdot \alpha_{C_4AF}(t) \cdot (C_4AF\%) + E \cdot (Blaine) + F \quad (1.7)$$

Shrinkage strain of the paste, ε_p , is depending on mineral degree of hydration, α_x , mineral content, $x\%$, and cement fineness, *Blaine*. *A* until *F* are constants and give most information. Constants for C_3S and C_2S are much smaller than those of C_3A and C_4AF and have a negative character. Therefore autogenous shrinkage is suggested to mainly depend on the hydration degree and relative amount of minerals C_3A and C_4AF .

1.5.2 Cement type

So far only hydration of OPC has been discussed. This research concerns CEM III/B, which consists for about 70% of BFS with a high Blaine value. While addition of BFS with low Blaine fineness slightly reduces autogenous shrinkage, fine BFS increases it, especially at large replacement ratios (Tazawa, 1998). Autogenous shrinkage of pastes with a 50% slag replacement was twice the size compared to OPC pastes (Hanehara et al., 1998). Hydrated blended slag cements show decrease in pore size and high discontinuity in the pore structure (Feldman, 1983), further enhancing self-desiccation. According to Chen [2006], most attention should be paid to slag reactivity and w/c . A low or medium levels of cement replacement by slag, there is only a minor influence on water restraintment by the hydration products. Chemical shrinkage may be significantly higher than in Portland cement and increases with higher slag content or high slag reactivity. With increasing slag proportions also gel and capillary porosity of the paste increase. Gel porosity is increased with increase of slag hydration degree, whilst capillary porosity decreases. Increasing w/c leads to a dramatic increase in capillary porosity.

Lura [2003] showed that shrinkage of pastes with BFS can only partially be explained by the capillary tension approach. Additional shrinkage was proposed to be caused by disappearance of internal restraints, due to consumption of CH crystals in the pozzolanic reaction of the slag. This reaction proceeds on the long term and even at reduced RH (Jensen, 1993).

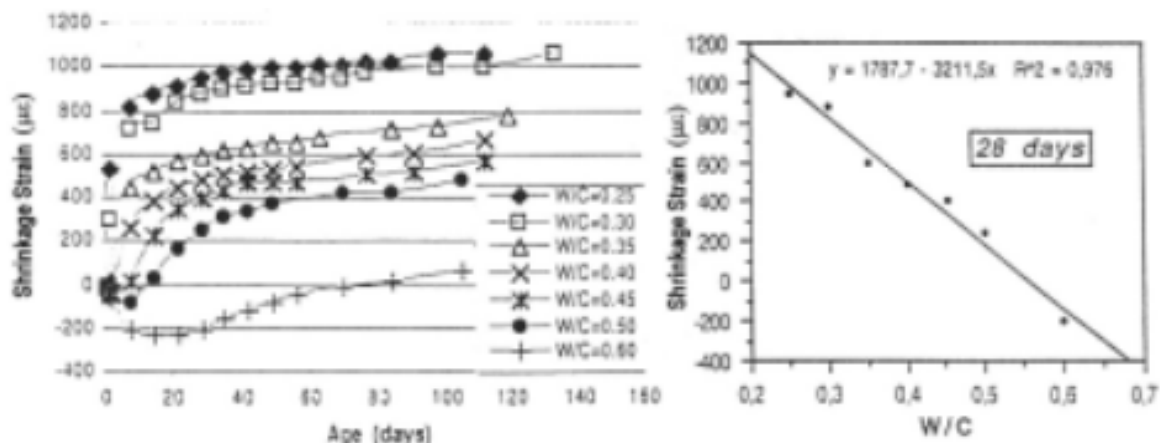


Figure 20 Correlation autogenous strain and w/c ratio for cement pastes, 28 days (Baroghel-Bouny, 1996)

1.5.3 Water / cement ratio

Powers & Brownyard [1948] stated that autogenous shrinkage due to self-desiccation occurs with a w/c ratio above 0.42, then all mixing water is consumed. Tazawa & Miyazawa [1995] attributed a denser paste structure to the increasing shrinkage with decreasing w/c . As w/c decreases, the initial spacing between particles decreases, denser structures lead to increasing magnitude of autogenous stresses induced by the menisci in partially filled capillaries. Expansive processes are also influenced by w/c , but are in case of lower w/c overwhelmed by the magnitude of the shrinkage (Bentz, 2009). Net autogenous shrinkage ($\varepsilon_{min-\varepsilon_{max}}$) values are found to monotonically decrease with increasing w/c . Figure 20 supports the hypothesis that lower w/c mixtures increase autogenous shrinkage (Baroghel-Bouny, 1996).

1.5.4 Superplasticizer

Plasticizers are used to increase workability, reducing yield stress. For a third generation SPL based on polycarboxylate ether, particles become better dispersed. A low dosage is already effective. Another influence is retardation of initial cement hydration and final setting by interactions with reactive species, affecting the hydration process for diffusion, nucleation and growth of hydrates, where higher doses have a more pronounced effect (Puertas et al., 2005). Early age microstructural changes regard pore size refinement and porosity reduction.

1.5.5 Aggregates

With the use of a stiff aggregate, strain reduction is expected. Since limestone has a higher stiffness than gravel (ROBK, 2006) reduction in shrinkage is expected. A similar influence may occur on the reduction of the maximum strain. Both according to Hooke:

$$\varepsilon_{t,max} = \frac{f_{t,spl}}{E_{mod}} \quad (1.8)$$

An equal stress, f_t , and a higher modulus of elasticity, E_{mod} , leads to a decrease in strain, ε_t .

1.5.6 Filler

While quartz powders are inert, limestone powders do not only act as nucleation sites, but are partly reactive, forming cementitious compounds. Hydration can be accelerated, so that hydration products quickly develop. At higher filler contents CH crystals are large and may bridge the space between particles (Pietersen, 1993). Particle size distribution of the filler lies close to that of cement, therefore the filler is not expected to act like an internal restraint.

1.5.7 Fibres

Fibres used in the fire resisting concrete are made of monofilament polypropylene. Polypropylene does not absorb water, since it is hydrophobic. Chemical bond is not expected, but mechanical interaction of the polypropylene fibres with the concrete matrix has been shown for fibrillated fibres. The elastic modulus is relatively low and may be a limiting factor. The fibres are used for early strength enhancement and increase of toughness. Because of the low melting point “relief channels” can be provided in case of high temperatures, because of disappearance of the fibres, relieving thermal and moisture stresses (ACI, 2002).

1.6 Reducing autogenous shrinkage

Methods for reduction of autogenous shrinkage are based on enhancing expansion processes, for instance by MSA (Chen, 2006), reducing surface tension of pore water, for instance by SRA and reduction of the capillary stresses, by internal curing.

Principle of internal curing is based on maximizing pore diameters and supplying additional water, for instance by LWA or SAP. A state of the art report on internal curing is supplied by NIST (Bentz & Weiss, 2011). Mixtures designed according to this current knowledge showed a substantially reduced autogenous shrinkage, but no total elimination. Especially when using blended cements autogenous shrinkage may not be eliminated by internal curing, since the shrinkage can partially be caused by the pozzolanic reaction between the supplementary material and calcium hydroxide, this loss of internal restraint leads to additional shrinkage (Jensen & Hansen, 1996) (Bentz, 2007).

1.7 Objectives of this thesis

So far autogenous shrinkage has been disregarded in case of normal strength concrete. There are signs that this may not be valid in case of BFS cement. Aim of the thesis is to provide insight and awareness regarding the relatively unknown subject of autogenous shrinkage, through investigating the influence of different material constituents and quantification of the relation of autogenous shrinkage to total shrinkage.

Objectives are to determine the magnitude of autogenous and drying shrinkage of concrete and relate it to each other. Point of entry is the commonly accepted hypothesis of capillary action as a mechanism of autogenous shrinkage. Influence is determined of constituents of the mixture on the size of autogenous shrinkage. Hereby the proportions of constituents are varied, as are the types of material. For pastes the autogenous shrinkage will be related to self induced stress under sealed conditions. General properties are determined both as control as to validate relevance for practice. Results of shrinkage experiments are compared to prediction models contained in norms for practice. Data from literature will be used for verification.

First part of the research considers autogenous and drying shrinkage of concrete specimens. Goal is to find out about difference in properties of the mixtures. Specifically when using limestone aggregate instead of gravel and addition of polypropylene fibres. Differences are determined in properties of dried out specimens compared to fully sealed specimens, regarding shrinkage and general properties in compression and tension. Comparison is made to practical guidelines for shrinkage in practice, contained in the codes.

Second part of the research considers pastes, where early age autogenous shrinkage is related to self induced stress under sealed conditions. Influence of cement and filler type and content is determined. Results from both parts combines behaviour of the pastes and concretes, leading to conclusions of practical relevance.

Chapter 2

Methods

In this chapter descriptions are presented for materials and test procedures used in this research. The test method for the Mini-TSTM is described in more detail, since this device is still under development. At the end of the chapter prediction models from practice are introduced, which will be used for comparative reasons.

2.1 Materials

Materials used in this research are based on concretes nowadays used in practice, therefore no detailed information is provided. All constituents are from the same batch, so that no material based difference should be expected.

2.1.1 Mixture designs

Table 1 shows the concrete mixture designs as applied in the research. Three types can be distinguished, where all types are executed with a water to cement ratio of both 0.50 and 0.45:

- Type T: Traditional mixtures, using gravel as coarse aggregate.
- Type N: Neutral limestone mixtures. Difference with type T is the use of limestone aggregate instead of gravel and the use of an additional limestone filler material.
- Type P: Polypropylene fibres are added to the type N mixtures. In practice this type of mixture is known as fire resisting concrete.

Table 2 gives the constituents of the cement pastes applied in the research. Mixture design is representative to the cement pastes in the used concrete material. Additional are OPC and an inert quartz filler material, both used for comparative reasons. The type of CEM I is chosen based on the Blaine value, being closest to that of the used CEM III/B. The type of quartz powder is chosen closest to the PSD and maximum particle size of the limestone powder. Product sheet information of the materials can be found in the appendix.

Table 1 Concrete mixtures

Concrete	T (0.50)	T (0.44)	1N	1P	2N	2P
Strength class	C28/35	C35/45	C28/35	C28/35	C35/45	C35/45
CEM III/B (kg/m ³)	340	340	340	340	360	360
LSP filler (kg/m ³)			20	20	20	20
Design w/c	0.50	0.44	0.50	0.50	0.46	0.46
SPL (% M/M _{cem})	0.2	0.2	0.2	0.4	0.2	0.4
Fine aggregate	Sand 0/4					
Coarse aggregate	Gravel	Gravel	Limestone	Limestone	Limestone	Limestone
Fractions	4/8, 8/16	4/8, 8/16	6/20	6/20	6/20	6/20
PP fibres (kg/m ³)				2		2

Table 2 Constituents cement paste mixtures

Cement paste		Additional information
Cement	340 kg/m ³	CEM I
		CEM III/B
Filler	6.5% V/V _{cem}	Extra CEM III/B (cem) Limestone powder (lsp) Quartz powder (qp)
Water	169 kg/m ³	gives w/c 0.50 and 0.46
Superplasticizer	0.5% V/V _{cem}	

2.1.2 Test programme

Table 3 shows the programme for experiments with concrete mixtures. Both prisms and cubes are used. Tests on prisms start on day 1 and run for 197 days in total. At 91 and 197 days general properties are determined for sealed prisms and unsealed prisms from 3 days.

Table 4 gives an overview on the experiments on the cement pastes. Free deformation and self induced stress tests are executed in the mini-TSTM, porosity is determined with MIP. Only one specimen is used per experiment, in case of CEM III two additional specimens are included for repeatability of deformation tests conducted with the mini-TSTM.

Table 3 Experiments concrete

Concrete	T (0.50)	T (0.44)	1N	1P	2N	2P	
Sealed shrinkage	2	2	3	3	3	3	
+ weight loss	1		1	1	1	1	
only weight loss			1	1	1	1	
Drying from 3 d.	2	2	3	3			
+ weight loss	1		1	1			
only weight loss			1	1			
Drying from 7 d.	2	2	3	3			
+ weight loss		1	1	1			
only weight loss			1	1			
Drying from 28 d.	2	2	3	3			
+ weight loss		1	1	1			
only weight loss			1	1			
Total prisms	10	10	20	20	5	5	70
Compr. strength 1 d.	1	3	4	4	3	3	
3 d.	1	3	4	4	3	3	
7 d.	3	1	4	4	3	3	
28 d.	3	1	4	4	3	3	
Total cubes	8	8	16	16	12	12	72

Table 4 Experiments cement paste

Cement paste	Free deformation	Restrained deformation	Porosity
CEM I	6 d.	6 d.	Y
CEM I + lsp	6 d.	6 d.	Y
CEM III	7 d., 4 d., 4 d.	7 d.	Y
CEM III + cem	7 d.	7 d.	Y
CEM III + lsp	7 d.	7 d.	Y
CEM III + qp	7 d.	7 d.	N

2.2 Testing procedures

Standards are available for the test methods on the concrete samples, among which mostly NEN-EN 12350 “Testing fresh concrete” and NEN-EN 12390 “Testing of hardened concrete” are used in this research. Different parts of the latter discuss specimens and moulds, manufacturing and storage and execution of strength tests. For the cement pastes in this research no standards are available, therefore a more thorough explanation is given.

2.2.1 Mixing and placing

All concretes are mixed and placed in the same way, as are the pastes. When the mixing procedure is finished the material is placed in a mould and compacted, all happens within half an hour from start of mixing.

In case of the fresh concrete general properties are determined, such as workability, air content and specific density of the material. This is done following the standard NEN-EN 12350 “Testing fresh concrete”. Water content is determined by NBN-EN 206-1. Compaction is done by means of a vibrating table. After casting the specimens are covered with plastic sheets to prevent early loss of water and kept at room temperature. Demoulding takes place after one day.

For the pastes the standard production procedure from ASTM C305 cannot be used, since the needed quantity of material is insufficient. Therefore special mixing tools are used (Figure 21). Pastes are mixed in a plastic bucket using a drilling machine with a special blade. As soon as the superplasticizer is fully activated and the mixture is stable, casting takes place through a cup with a needle. Where needed pastes are compacted using a milk frother with the head cut off. Next the specimen is sealed with a plastic foil and covered with an aluminium foil in order to prevent drying.



Figure 21 Paste production: Mixing device (l), cup for pouring (m), vibrating device (r)

2.2.2 Compressive and tensile splitting strength

For determining the compressive strength of the concrete material according to the set norms, in total 72 cubes of size $150 \times 150 \times 150 \text{ mm}^3$ are produced. After demoulding, the cubes are placed in a climatized room and kept at a relative humidity of almost 100% and a temperature of around 20°C . Compressive strength is determined at age of 1, 3, 7 and 28 days.

Furthermore, compressive and tensile splitting strength are determined at day 91 and 197. Hereby specimens are cut from the prisms used in the shrinkage tests, to determine the properties of uncured material. From each prism three cubes of size $100 \times 100 \times 100 \text{ mm}^3$ are extracted.

Testing procedure is executed according to NEN-EN 12390 “Testing of hardened concrete”, where part 4 gives specifications for testing machines for compressive strength.

2.2.3 Modulus of elasticity

The elastic modulus is determined in compression on day 91 and 197. Specimens used are prisms of size $400 \times 100 \times 100 \text{ mm}^3$ and come from the tests determining autogenous shrinkage and drying shrinkage from 3 days (Figure 22r). Tests are deformation controlled and performed in the Schenk 7596, a standard apparatus for material testing. First the prism is loaded until approximately 40% of the compressive strength, then unloaded and reloaded to let the measuring equipment set, when the stress-strain curve is linear loading continues until failure. Elastic moduli are determined by means of the secant modulus.

2.2.4 Porosity

Porosity of cement pastes is determined by aid of the Mercury Intrusion Porosimeter (MIP). Pastes were cast in small tubes and stored for 28 days. After demoulding samples were dry cut from the centre and freeze dried for several weeks. In the MIP mercury is pushed into the samples, filling up the empty pores. The pressure at which this occurs determines the pore size, the pushed in volume of mercury at the given pressure gives the pore volume. Using weight changes additional properties can be determined, such as bulk and skeletal densities.

2.2.5 Autogenous and drying shrinkage concrete

In total 70 prisms are produced, each of size $400 \times 100 \times 100 \text{ mm}^3$. After demoulding the prisms are directly wrapped in plastic foil and sealed with aluminium foil to prevent moisture exchange with the surrounding environment. Afterwards the prisms are placed in a climatized room, where the temperature ($20^\circ\text{C} \pm 2^\circ\text{C}$) and relative humidity ($50\% \pm 2\%$) are kept constant.

In case of drying shrinkage the prisms are unsealed in the length of the specimen (Figure 22l), to enable moisture exchange with the surrounding environment. Specimens are unsealed respectively 3, 7 or 28 days after casting.

To determine the size of the shrinkage, length change is measured per accompanying prism. This is done by attaching a measuring device (“clock”) at two opposite sides of the prism, with a measuring length of 20 cm and an accuracy of $1 \mu\text{m}$ (Figure 22l).



Figure 22 Test for shrinkage with “clocks” (l) and modulus of elasticity (r)

Weight loss is determined by weighing accompanying prisms on an electric scale with an accuracy of 0.1 gram. Weighing is executed at times of readings on the measuring devices. Also sealed specimens are weighed, in order to check for moisture exchange. Water transport through the foils may be possible and should be verified, in order to determine the significance of the occurring error for the autogenous measurements.

From the start measurements are taken every day at the same time, excluding the weekend. In case the difference in magnitude is smaller than 0.1 μm , the time in between measurements doubles.

2.2.6 Autogenous deformation and self-induced stresses in paste

Autogenous shrinkage can be measured volumetrically or linearly. Detailed investigation on several methods suggested the volumetric method by means of immersion of a latex membrane to be inappropriate, due to water ingress through the membrane during the test (Lura & Jensen, 2005). Also reabsorption of bleeding water can be erroneously measured as shrinkage. In linear methods this may be seen as an increased expansion. Even though there is no standardized method for autogenous deformation of cement pastes and mortars, the linear method is opted for standardization by an ASTM committee.

In this research a relatively new linear method will be used, based on a scaled down version of the TSTM for concretes. The TSTM is an internationally recognized method for linear measurements regarding tests involving uni-axial tension on early-age concrete (RILEM, 1982). Additional information on the design, development and assembly of the Mini-TSTM can be found in a previous Master dissertation (Leegwater, 2006).

Basis for the Mini-TSTM is the mini tensile test setup, with total dimensions that fit on half of an A4 paper. The tensile test setup is designed to fit inside the ESEM, so that progress of tests can be monitored through the electron microscope. Because of the vacuum inside the ESEM chamber this is not possible for materials used in the Mini-TSTM, such as pastes of early age.

The Mini-TSTM will be used to measure free deformation and self-induced stress of pastes and fine mortars under autogenous conditions for several subsequent days. After finishing the test, the specimen is deliberately cracked in order to obtain a stress-strain diagram.

Linear methods can have a problem in restraining the cement paste. Figure 24 shows the several parts of which the Mini-TSTM setup consists. In order to reduce friction bottom and side parts of the mould of the Mini-TSTM are made out of Acetal (nr. 5, 6), which is a synthetic polymer material. Furthermore the stainless steel end plates are lubricated (nr. 2, 4). The stainless steel wedge-shaped parts (nr. 3) are kept without lubrication to enable transferring tension without slip of the specimen.

The wedge-shaped parts can introduce or can be subjected to a longitudinal tensile force, at one end of the device these parts are connected to the load cell. The compressive force is taken up by the end plates.

Autogenous conditions are created by covering the mould first with a plastic sheet and then with an aluminium sheet. To create a watertight connection without friction a Vaseline lubricant is used in between the cover and the mould. Because of the size of the specimen, tests performed will be isothermal.

Deformations can be measured using the LVDT attached to the tensile test setup, but is also sensitive to deformations occurring in the tensile testing device, including the load cell. Therefore the linear deformations are measured using an additional extensometer (Figure 23). The extensometer measures the change in distance between two stainless steel claws, connected to the two wedge-shaped parts. Besides a support for the extensometer, the claws work as a prestress on the two wedge-shaped parts, limiting deformation when a force is exerted on them.

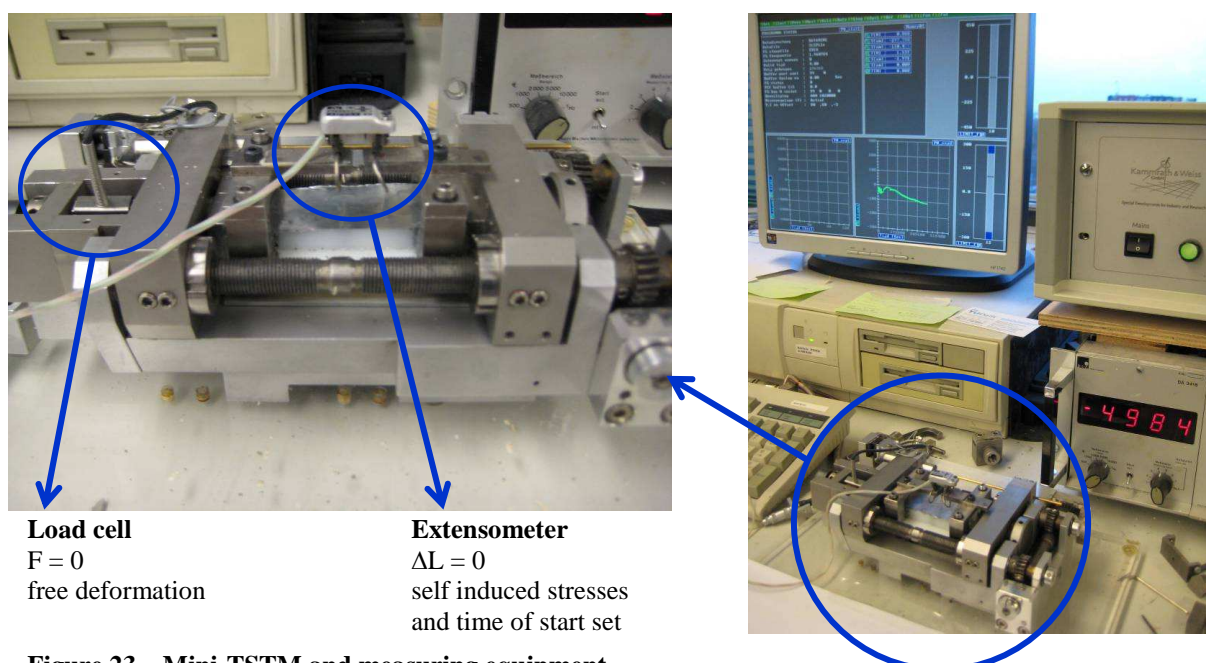


Figure 23 Mini-TSTM and measuring equipment

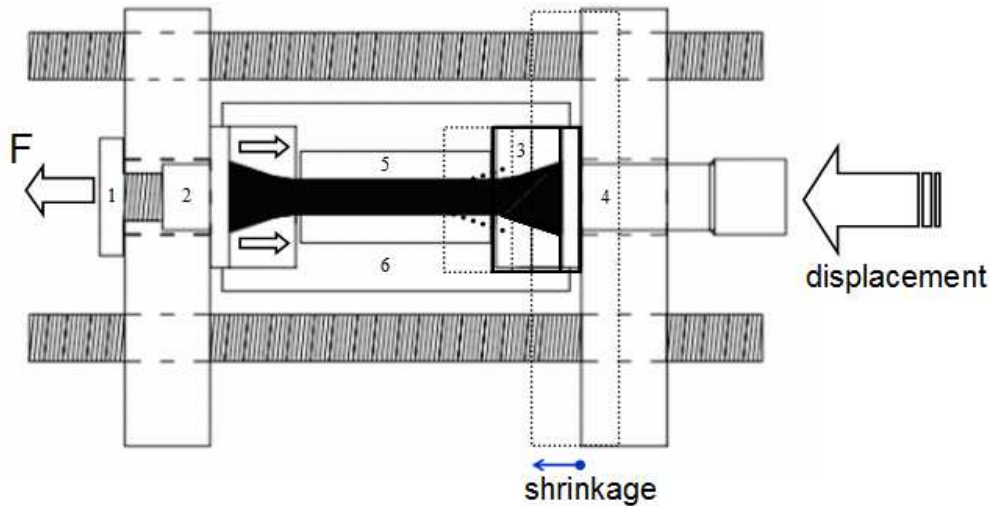


Figure 24 Working of Mini-TSTM

Data acquisition is done by aid of a personal computer. The software stores the scanning of the amplifier and generates functions for deformation or force control. Next to the load cell, both the LVDT of the device as the extensometer are connected to the amplifier. All can be used for control.

Because deformations are constantly adjusted, the motor of the device will be turned on at all times. For deformation controlled tests the measured change in deformation of the specimen remains zero. When shrinkage occurs, the device pulls on the specimen by opening, keeping the change in deformation on zero.

In case of a load controlled test, the load has to remain zero throughout the test. If the specimen shrinks, a tensile force is measured. The tensile test setup closes, so that the load is zero again (Figure 24).

Measurements can commence directly after casting, even in case of fresh paste. Time zero for autogenous deformation can be determined afterwards, using results of the self-induced stress tests. Initial upbuilt of stress in the specimen determines initial set and therefore onset of autogenous deformation in the free deformation test.

In case the specimen does not crack during the test, it is deliberately cracked under deformation control after the test finishes. The same strain rate is chosen as in the modulus of elasticity tests performed on the concrete samples.

2.3 Models

Prediction models are used for comparison with the results found in the concrete experiments. Blended slag cement is mainly used in The Netherlands and Japan, therefore the standard specifications valid in these countries are taken as reference, EuroCode and the code by JSCE. Both models are based on Portland cement, but in Japan a factor is included for cement type.

2.3.1 EuroCode

Both autogenous and drying shrinkage can be calculated according to NEN-EN 1992-1-1.

$$\varepsilon_{cs} = \varepsilon_{cd} + \varepsilon_{ca} \quad (2.1)$$

Superposition of drying, ε_{cd} and autogenous shrinkage, ε_{ca} , gives the total shrinkage strain, ε_{cs} (Figure 25). Where autogenous shrinkage is calculated according to the following equation:

$$\varepsilon_{ca}(t) = \beta_{as}(t) \cdot \varepsilon_{ca}(\infty) \quad (2.2)$$

Depending on characteristic compressive strength and time:

$$\varepsilon_{ca}(\infty) = 2.5 \cdot (f_{ck} - 10) \cdot 10^{-6} \quad (2.3)$$

$$\beta_{as}(t) = 1 - \exp(-0.2 \cdot t^{0.5}) \quad (2.4)$$

Drying shrinkage is estimated as follows:

$$\varepsilon_{cd}(t) = \beta_{ds}(t, t_s) \cdot k_h \cdot \varepsilon_{cd,0} \quad (2.5)$$

Depending on a nominal value for unrestrained drying shrinkage through $\varepsilon_{cd,0}$ and the notional size h_0 through k_h and in β_{ds} combined with time, t , and time of start drying, t_s .

$$\beta_{ds}(t, t_s) = \frac{t - t_s}{(t - t_s) + 0.04 \cdot \sqrt{h_0^3}} \quad (2.6)$$

Table 5 shows the values for the parameters in the EuroCode, in order to predict shrinkage behaviour of the concrete specimens in the executed research.

Table 5 Values parameters in EC for concrete mixtures

EC factors		C28/35	C35/45
f_{ck}	[N/mm ²]	35	45
$\varepsilon_{ca}(\infty)$	[$\mu\text{m}/\text{m}$]	50	62.5
$\varepsilon_{cd,0}(\infty)$	[$\mu\text{m}/\text{m}$]	0,49	0,45
h_0	[mm]	50	(= $2 \times 100^2 / 4 \times 100$)
k_h		1	
t_s	[d]	3, 7, 28	

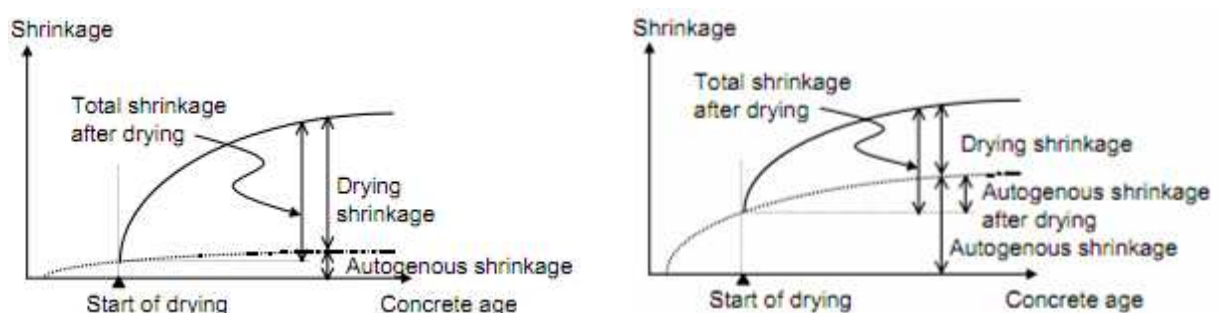


Figure 25 Shrinkage in conventional (l) and high-strength (r) concrete (Sakata & Shimomura, 2004)

2.3.2 Japan Society of Civil Engineers (JSCE)

For normal strength concrete, with compressive strength until 55 N/mm^2 , the 1996 Japan code gives a total shrinkage, consisting only of drying shrinkage (Sakata & Shimomura, 2004):

$$\varepsilon'_{cs}(t, t_0) = \left[1 - \exp\left\{-0.108(t - t_0)^{0.56}\right\} \right] \cdot \varepsilon'_{sh} \quad (2.7)$$

The total shrinkage depends on time, t , time of start drying, t_0 and through factor ε'_{sh} on the external humidity, RH , water content of the mix, W , and the volume over surface ratio, V/S :

$$\varepsilon'_{sh} = -50 + 78 \left[1 - \exp(RH / 100) \right] + 38 \log_e W - 5 \left[\log_e (V / 10S) \right]^2 \quad (2.8)$$

Autogenous deformation is included in the 2002 Japan code, for $0.20 \leq w/b \leq 0.65$ and based on mineral composition (Tazawa, 1998). Extensive research is done on Portland cement, influence of other cement types is momentarily based on regression analysis. Prediction of autogenous shrinkage according to the JSCE Specification 2002 is as follows:

$$\varepsilon_c(t) = \gamma \cdot \varepsilon'_{as,\infty} \cdot \beta(t) \quad (2.9)$$

With factors for type of cement, γ , water to cement ratio, w/c , through $\varepsilon_{as,\infty}$ and $\beta(t)$ and time, t , and time of setting, t_s , through $\beta(t)$:

$$\varepsilon'_{as,\infty} = 3070 \exp\{-7.2(W / C)\} \quad 0.2 \leq w/b \leq 0.5 \quad (2.10a)$$

$$\varepsilon'_{as,\infty} = 80 \quad 0.5 < w/b \quad (2.10b)$$

$$\beta(t) = 1 - \exp\left[-a(t - t_s)^b\right] \quad (2.11)$$

Miyazawa & Tazawa [2005] proposed the following equations for determining factors a and b :

$$a = 3.27 \exp\{-6.83 \times (w / c)\} \quad (2.12)$$

$$b = 0.251 \exp\{2.49 \times (w / c)\} \quad (2.13)$$

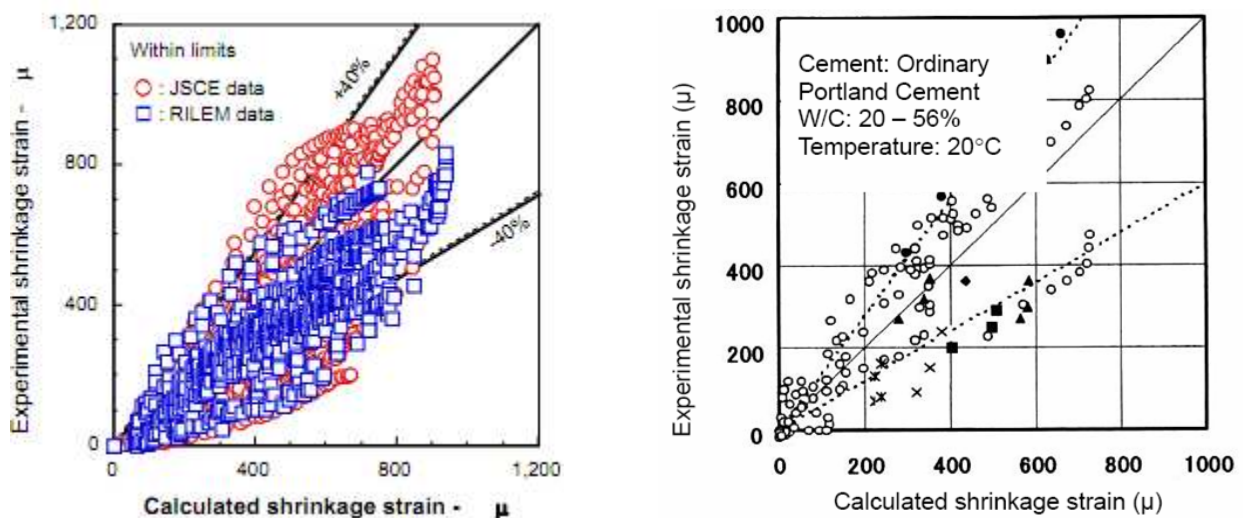


Figure 26 Left: Verification of total shrinkage in JSCE Specification 1996, data from JSCE and RILEM, for concrete with $f'_c < 80 \text{ N/mm}^2$ (Sakata & Shimomura, 2004)
 Right: Verification of autogenous shrinkage in JSCE Specification 2002 (Tazawa, 1999)

JSCE prediction models have been verified using data from RILEM and JSCE, both for the total shrinkage as for the autogenous shrinkage (Figure 26), showing good correlation ($\pm 40\%$).

Table 6 shows the values for the parameters in the JSCE prediction model, in order to predict shrinkage behaviour of the concrete specimens in the executed research.

Table 6 Values parameters in JSCE for concrete mixtures

JSCE total shrinkage		wcr 0.45	wcr 0.50
ε'_{sh}	[$\mu\text{m}/\text{m}$]	89.23	90.14
RH	[%]	50	
W	[kg/m^3]	165	169
V/S	[mm]	25	(= $400 \times 100^2 / 4 \times 100 \times 400$)
γ		1	
t₀	[d]	3, 7, 28	
JSCE autogenous		wcr 0.45	wcr 0.50
W/C		0.45	0.50
$\varepsilon_{as,\infty}$	[$\mu\text{m}/\text{m}$]	113.23	85.68
a		0.14	0.11
b		0.79	0.87
t_s	[d]	0	

Chapter 3

Results

This chapter presents the results of the conducted experiments. First are the concrete experiments, with a comparison to practical models, followed by the experiments on cement paste. Eventually main findings on concrete and cement paste are combined.

3.1 Concrete general properties

3.1.1 Compressive strength

Table 7 gives the compressive strength tests for all six mixtures after 1, 3, 7 and 28 days.¹ Figure 27 gives a graphical representation of the compressive strength development per mixture, until 197 days. Results on day 91 and 197 are from tests on cut prisms from sealed and unsealed (3D) experiments. The limestone mixture with higher wcr (1N) even has a higher strength than the fibre mixture with lower wcr (2P). Difference between limestone and fibre mixtures of the same wcr is about 10%. Strength reduction upon drying from 3 days is 10 to 20 % compared to sealed specimens of the same mixture.

Table 7 Results compressive strength

Mixture		Compressive strength [MPa]			
Code	Description	1d	3d	7d	28d
T (0.50)	Traditional – gravel aggregate	8.10	17.41	31.45	47.14
T (0.44)	Traditional – gravel aggregate	10.38	22.12	36.32	51.84
1N (0.50)	Limestone aggregate	7.00	22.23	36.24	51.04
1P (0.50)	Limestone + PP fibres	6.91	21.89	32.98	44.13
2N (0.46)	Limestone aggregate	11.28	26.97	42.81	57.49
2P (0.46)	Limestone + PP fibres	6.31	22.46	36.68	48.24

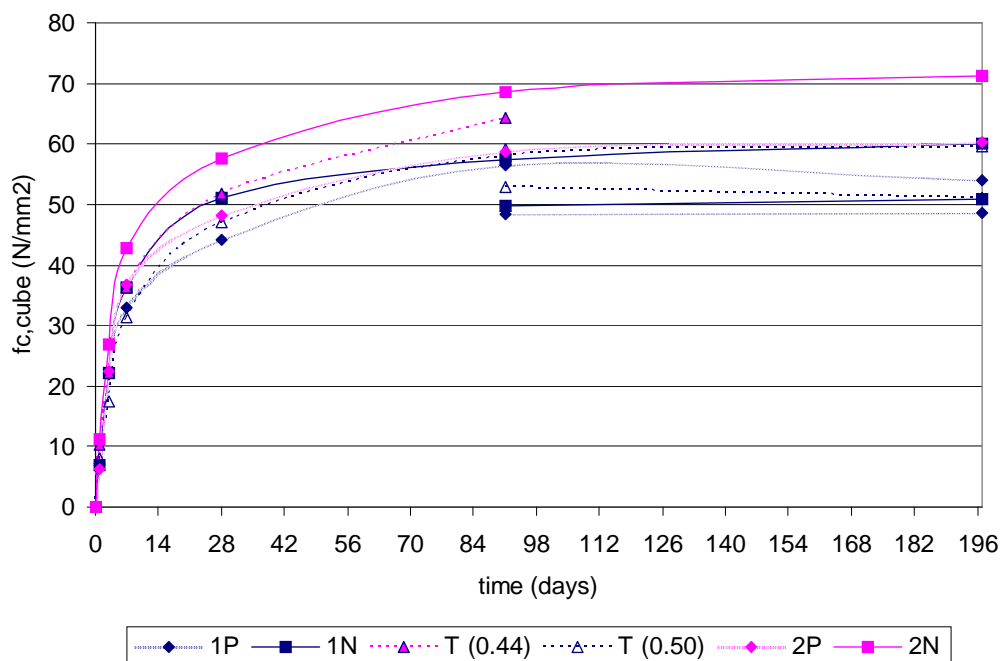


Figure 27 Results compressive strength, where:
P = fibre mixture, N = limestone mixture, T = traditional mixture

¹ N.B.: From EuroCode the mean compressive strength at 28 days is given, 43 MPa and 53 MPa for mixtures respectively with wcr \approx 0.50 (C28/35) and wcr \approx 0.45 (C35/45).

3.1.2 Maximum strain

Table 8 shows measured general properties on specimens from prisms at day 91 and 197. Specimens are kept fully sealed until that day or are unsealed from day 3 and exposed to drying. No significant differences are found for compressive strength measurements, other than that strength of the prism is about 75% of the strength of the cube, which correlates with values from the EuroCode. The ratio of tensile splitting strength to modulus of elasticity gives an approximation of the elongation at break. In case of limestone aggregates tensile splitting strength is lower than for traditional concrete (T) and the modulus of elasticity is higher. This leads to a reduction in elongation at break of around 10%.

Table 8 General properties sealed and unsealed prisms, day 91 and 197, A = sealed, 3D = drying from 3 days

Compressive strength Prisms		f_c [N/mm²]					
		P 91d	P 197d	N 91d	N 197d	T 91d	T 197d
wcr 0.50	A	42.88	45.22	39.71	42.80	44.67	
	3D	35.56	44.58	34.73	36.04	40.48	
wcr 0.45	A	46.33	47.14	48.25	52.30	49.21	
	3D					43.68	
Compressive strength Cubes		f_c [N/mm²]					
		P 91d	P 197d	N 91d	N 197d	T 91d	T 197d
wcr 0.50	A	56.38	54.08	57.44	59.99	58.02	59.61
	3D	48.50	48.69	49.67	50.80	52.95	51.00
wcr 0.45	A	58.64	60.32	68.54	71.29	64.29	
	3D					59.06	
Tensile splitting strength Cubes		$f_{t,pl}$ [N/mm²]					
		P 91d	P 197d	N 91d	N 197d	T 91d	T 197d
wcr 0.50	A	3.92	4.06	4.62	3.90	4.65	4.77
	3D	3.89	3.78	4.06	4.04	4.63	4.45
wcr 0.45	A	4.41	4.30	4.37	4.16	5.67	
	3D					4.38	
Modulus of Elasticity Prisms		E_c [N/mm²]					
		P 91d	P 197d	N 91d	N 197d	T 91d	T 197d
wcr 0.50	A	41.72	41.87	44.91	46.47	40.94	
	3D	32.93	32.40	38.09	33.79	35.58	
wcr 0.45	A	42.77	43.16	45.93	44.21	42.28	
	3D					36.50	
Elongation at break Cube/Prism		ϵ_t [$\mu\text{m}/\text{m}$]					
		P 91d	P 197d	N 91d	N 197d	T 91d	T 197d
wcr 0.50	A	93.84	97.09	102.78	83.85	113.59	
	3D	118.03	116.62	106.71	119.46	130.26	
wcr 0.45	A	103.15	99.56	95.09	94.18	134.16	
	3D					120.01	

3.2 Concrete shrinkage

Results for shrinkage experiments are shown until 91 days. From that day part of the specimens have been used in determination of general properties. Tests ran until a maximum of 197 days, these additional results are included in the appendix. A single line gives the average value for measurements conducted on the accompanying prisms.

3.2.1 Weight loss

Figure 28 shows the weight loss per prism for the drying experiment. In case of drying from 3 days the weight loss of the traditional mixtures (T) is comparable to that of the limestone mixture (N). The fibre mixture (P) has a reduced weight loss when compared to the other mixtures. In case of drying from 7 and 28 days this cannot be seen, for which an explanation is not readily available.

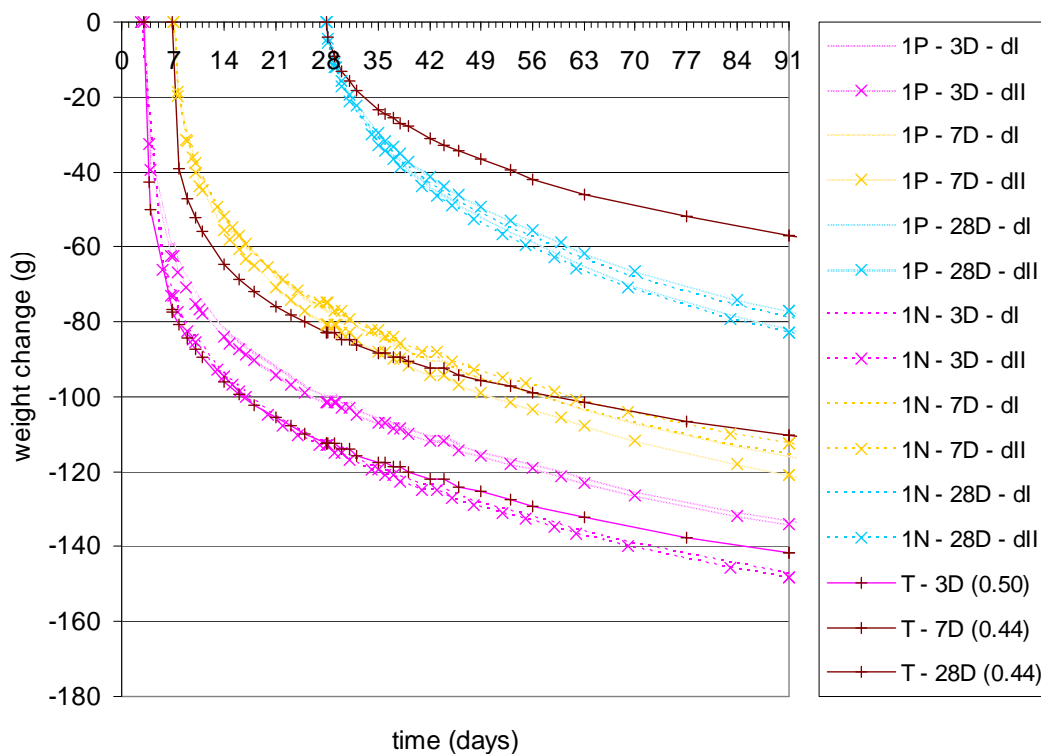


Figure 28 Weight loss specimens undergoing drying as a function of time, where:

1P = fibre mixture, 3D = drying from 3 days,
 1N = limestone mixture, 7D = drying from 7 days,
 T = traditional mixture, 28D = drying from 28 days,
 dI, dII = specimen number.

3.2.2 Total shrinkage

Figure 29 shows the development of the total shrinkage in time, as a combination of sealed and drying shrinkage. A single line is the average of the measurements conducted on prisms belonging to the specific test. The traditional mixtures (T) show a higher drying than the other mixtures. It is particularly notable for drying from 3 days. Total shrinkage when the concrete is dried out from 3 days consists for approximately 50% of sealed shrinkage.

Figure 30 and Figure 31 regard a comparison of total shrinkage measurements. When total shrinkage is separately considered per mixture, it is shown that the line of sealed shrinkage is followed until the specimens are exposed to drying.

Figure 30 contains measured total shrinkage of both traditional mixtures with a w/c of 0.44 and 0.50, a higher w/c shows higher drying shrinkage and therewith higher total shrinkage.

Figure 31 contains measured total shrinkage of limestone concrete both with and without fibres, in case of drying from 3 days the drying shrinkage is equal for limestone with and without fibres. In case of drying from 7 and 28 days this difference is not visible, for which an explanation is not readily available.

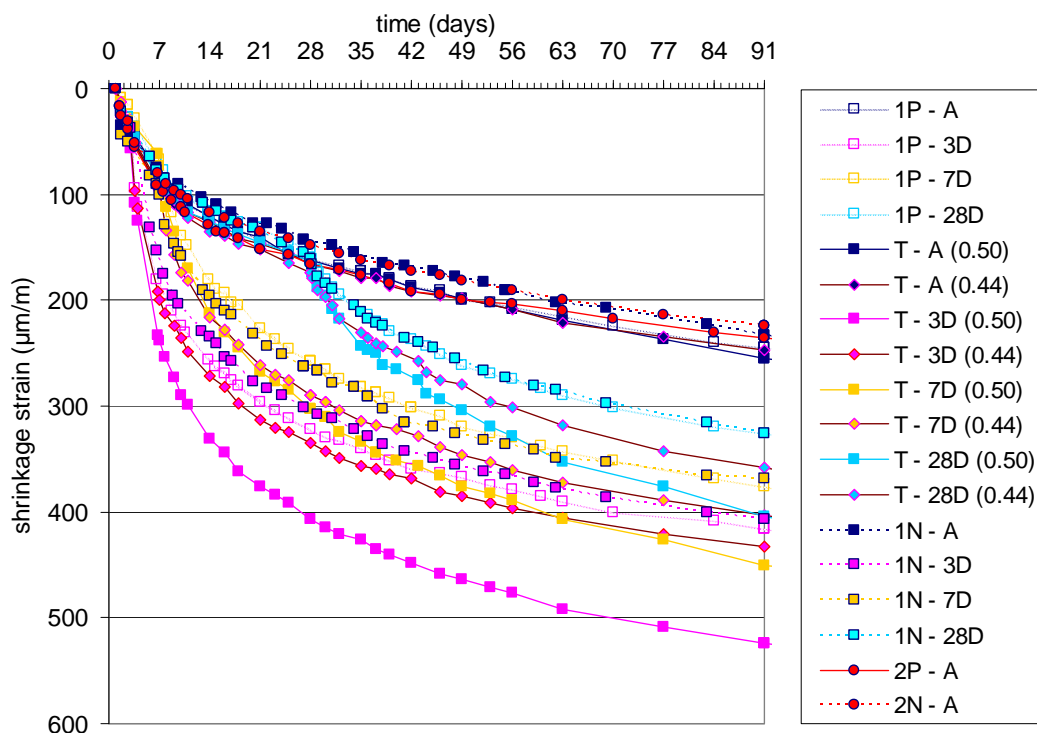


Figure 29 Results total shrinkage measurements, where:
P = fibre mixture, A = sealed,
N = limestone mixture, 3D = drying from 3 days,
T = traditional mixture, 7D = drying from 7 days,
28D = drying from 28 days.

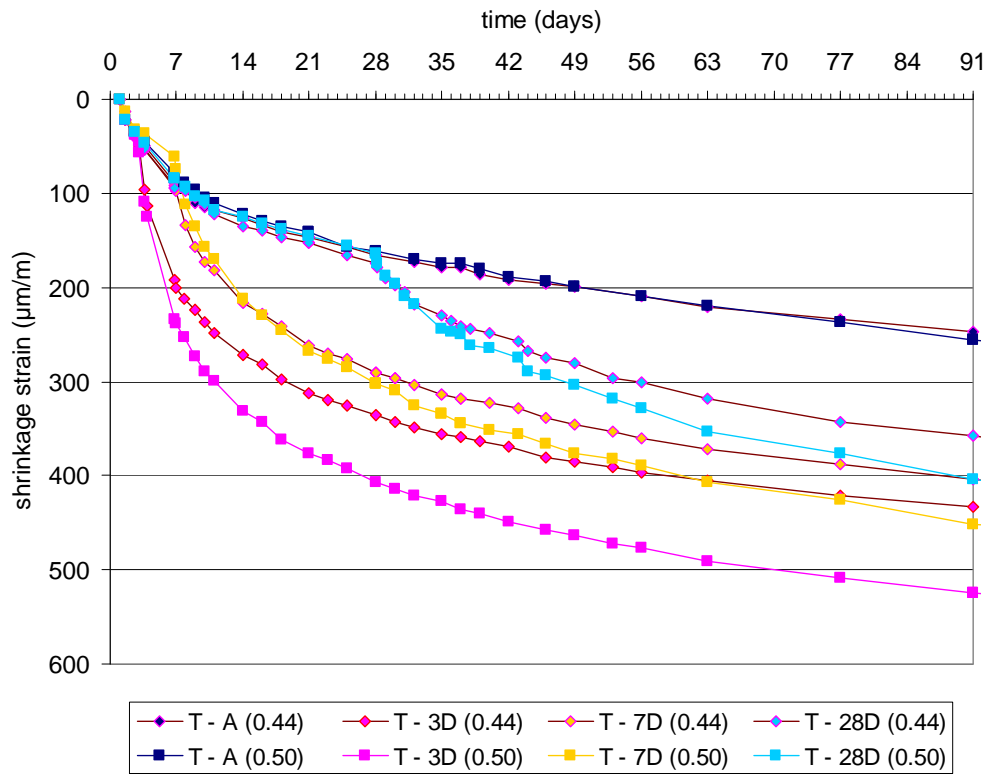


Figure 30 Total shrinkage traditional mixtures, wcr \approx 0.50 (square) and 0.45 (diamond), where:
 A = sealed, 3D, 7D, 28D = drying, respectively from 3, 7 or 28 days

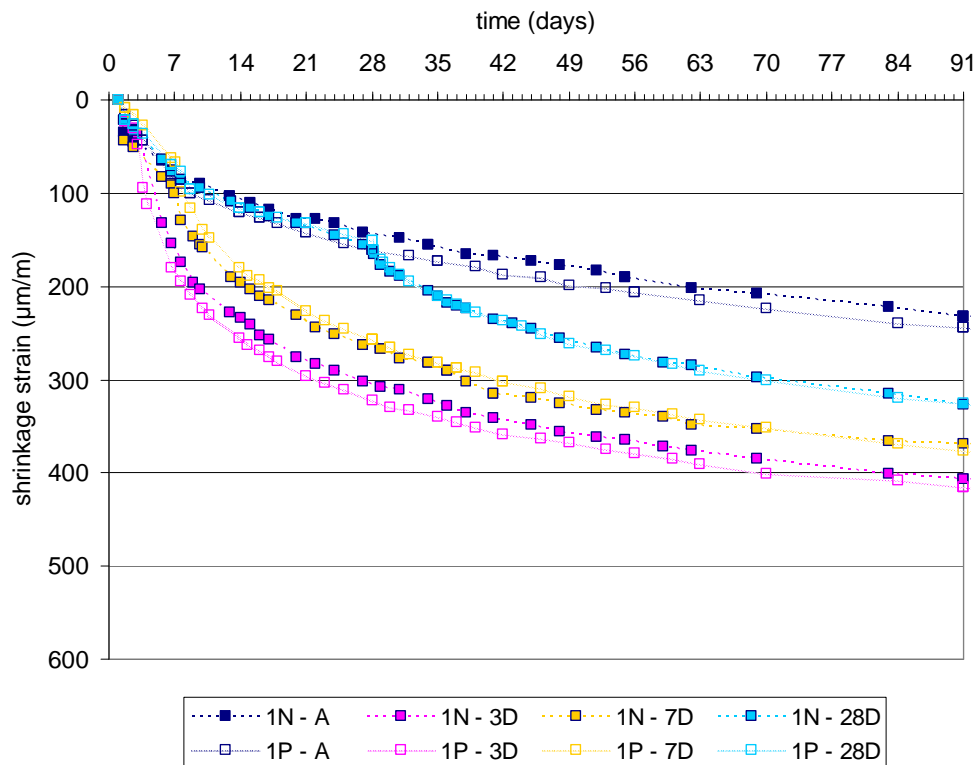


Figure 31 Total shrinkage limestone mixture (dashed line) en fibre mixture, wcr \approx 0.50, where:
 A = sealed, 3D, 7D, 28D = drying, respectively from 3, 7 or 28 days

3.2.3 Drying shrinkage and weight loss

Figure 32, Figure 33 and Figure 34 show total shrinkage strain versus weight change for accompanying specimens, starting from respectively 3, 7 and 28 days. All mixture types show a linear relation in time. For the first days a significant weight change is observed, while only little shrinkage occurs, the time in which this happens becomes shorter when drying starts from a later age. This initial weight loss may be contributed to evaporation of free water, supported by visual observation upon unsealing of the specimen. In minutes a relatively quick drop in mass was witnessed, accompanied by colour change of the specimen from white to dark grey and back to a light colour.

Total weight change reduces when the specimens are unsealed from a later age, so does the ratio of shrinkage strain. For drying from 3 and 7 days, fibre concrete (P) shows a substantial reduction in ratio of shrinkage strain to a given weight loss, around 40% when compared to traditional concrete (T). For limestone concrete (N) the reduction is around 10~15%. For drying from 28 days reduction in shrinkage ratio is about 25 and 40% for respectively fibre concrete (P) and limestone concrete (N).

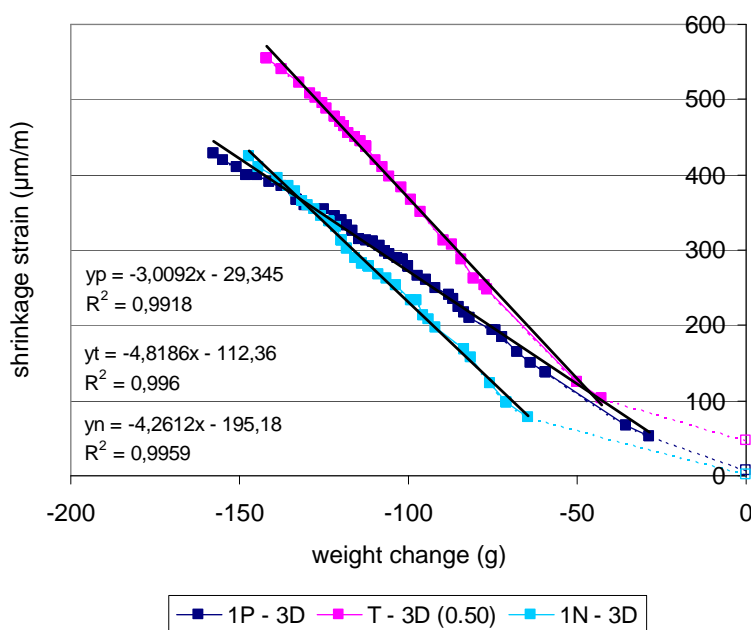


Figure 32 Total shrinkage strain versus weight change unsealed specimens from 3 days, where: P = fibre mixture, N = limestone mixture, T = traditional mixture

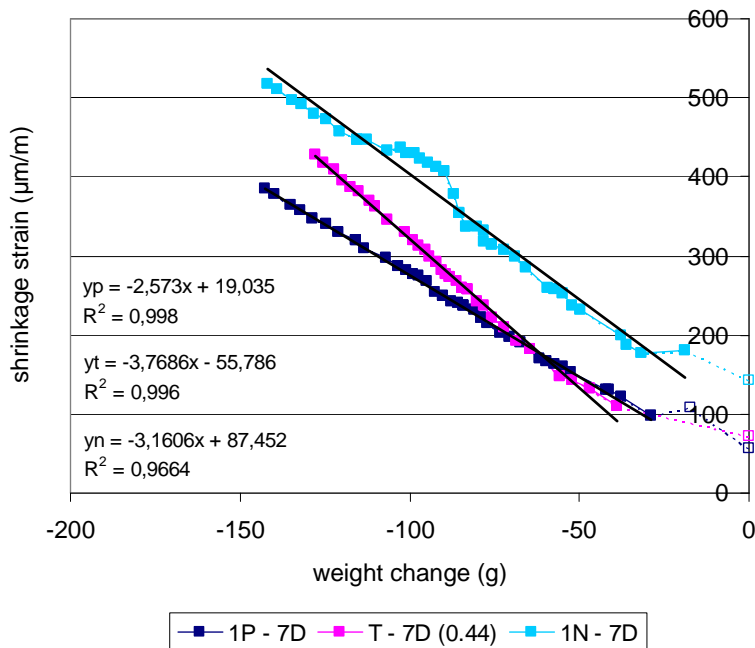


Figure 33 Total shrinkage strain versus weight change unsealed specimens from 7 days, where: P = fibre mixture, N = limestone mixture, T = traditional mixture

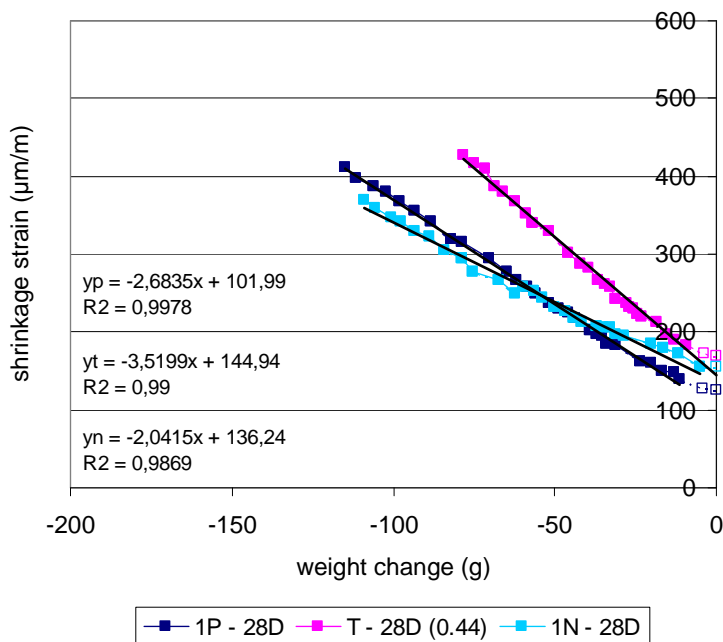


Figure 34 Total shrinkage strain versus weight change unsealed specimens from 28 days, where: P = fibre mixture, N = limestone mixture, T = traditional mixture

3.2.4 Sealed shrinkage

Measurements of sealed shrinkage are separately considered in this paragraph.

Figure 35 shows a comparison of sealed shrinkage measurements for the three mixtures with a wcr around 0.50. Upon application of limestone aggregates a lower shrinkage occurs when compared to the mixtures with gravel aggregates. Course of the shrinkage for fibre concrete is comparable to that of the traditional mixture. The shrinkage reducing effect of the limestone aggregate seems negated by addition of fibres. Figure 36 shows a similar image for the mixtures with lower wcr (≈ 0.45).

Figure 37 shows the sealed shrinkage of both traditional mixtures, with wcr 0.44 en 0.50. Shrinkage at a lower wcr is slightly higher, but the difference is small. The water to cement ratio seems of little effect (between wcr 0.44 and 0.50).

Figure 38 compares sealed shrinkage of both fibre mixtures and limestone mixtures. Also here the difference in wcr seems of limited influence. Shrinkage is slightly higher with lower wcr. Addition of fibres gives a modest increase in sealed shrinkage of the concrete.

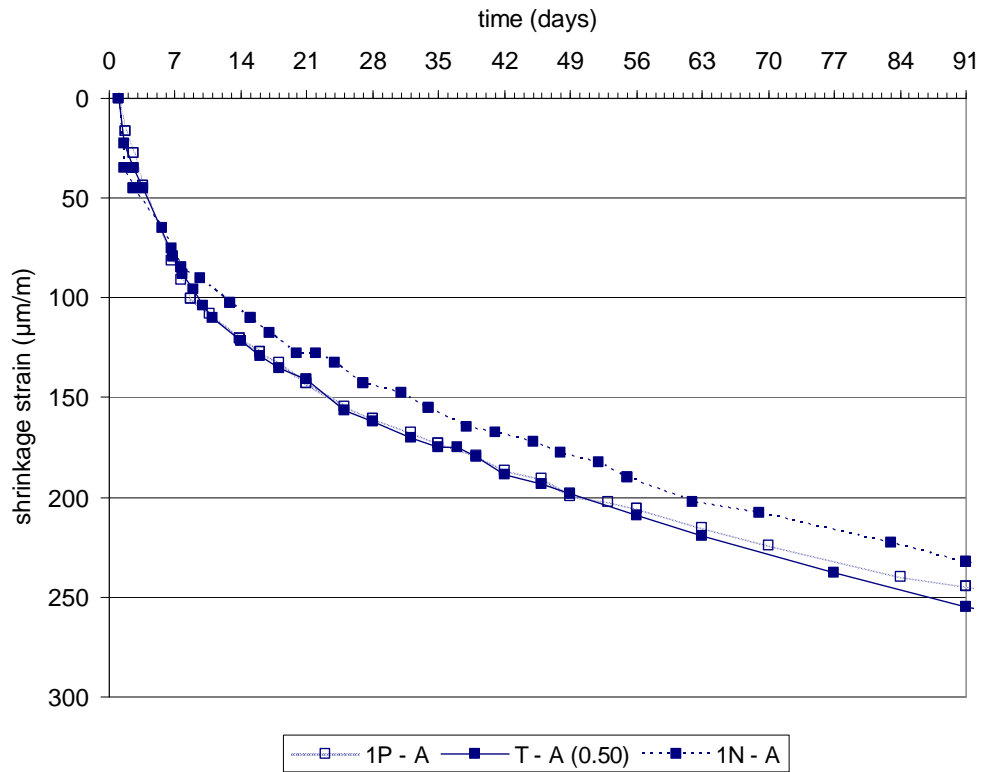


Figure 35 Sealed shrinkage, mixtures with higher wcr (≈ 0.50), where:
 P = fibre mixture, N = limestone mixture, T = traditional mixture

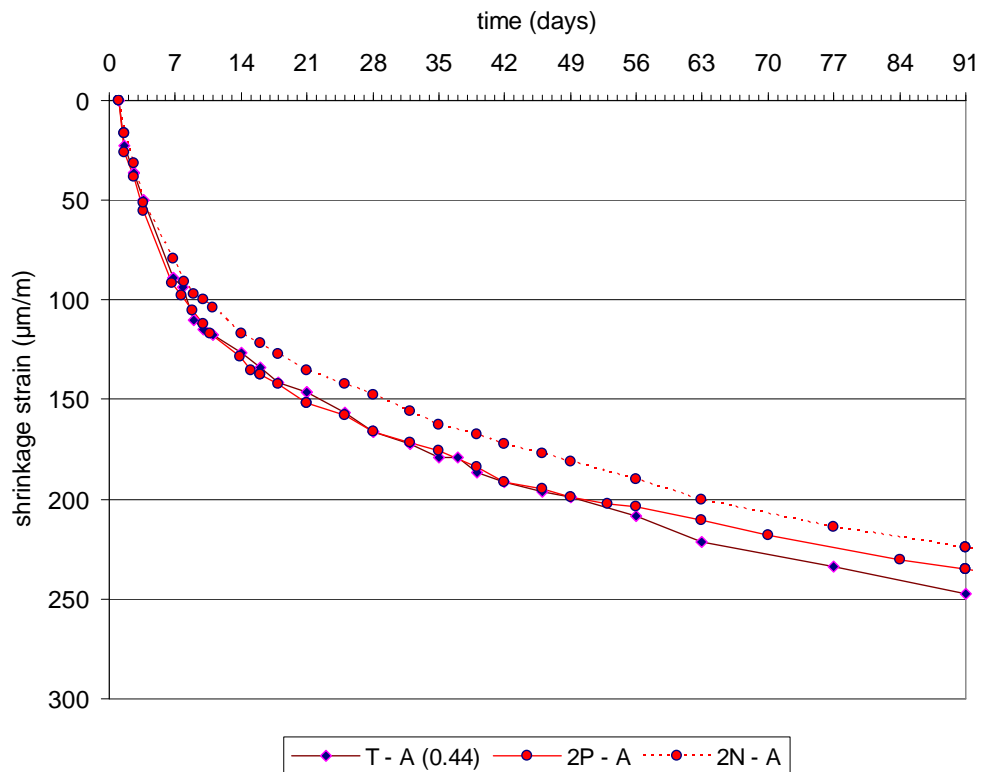


Figure 36 Sealed shrinkage, mixtures with lower wcr (≈ 0.45), where:
 P = fibre mixture, N = limestone mixture, T = traditional mixture

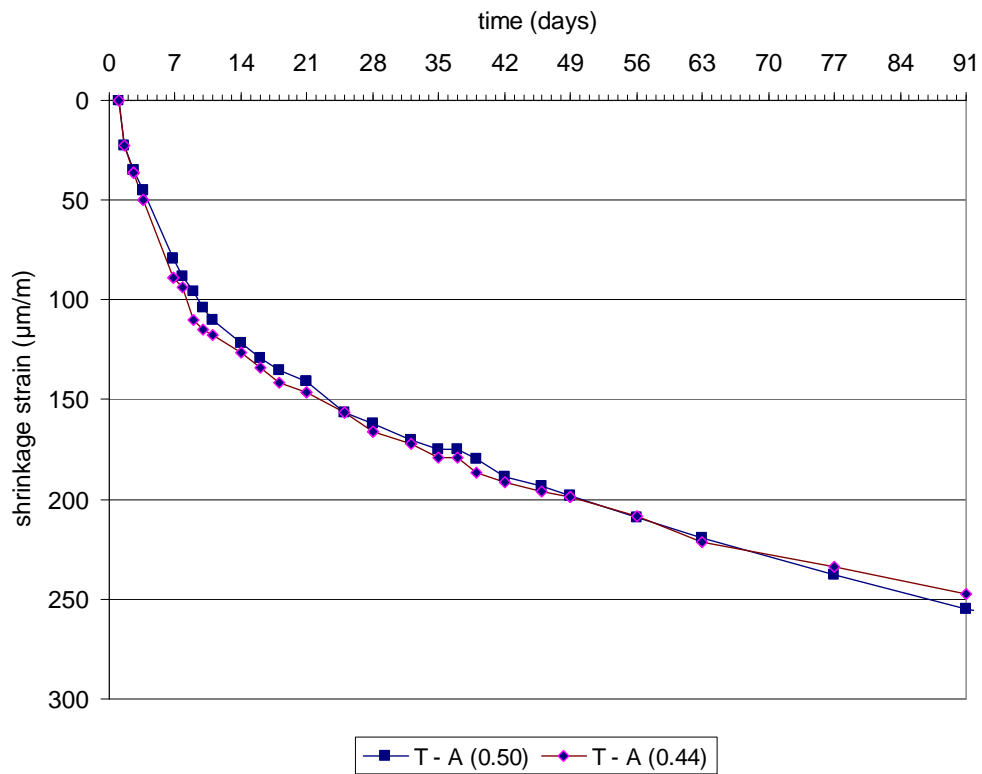


Figure 37 Sealed shrinkage, both traditional mixtures, wcr \approx 0.50 (blue) and 0.45

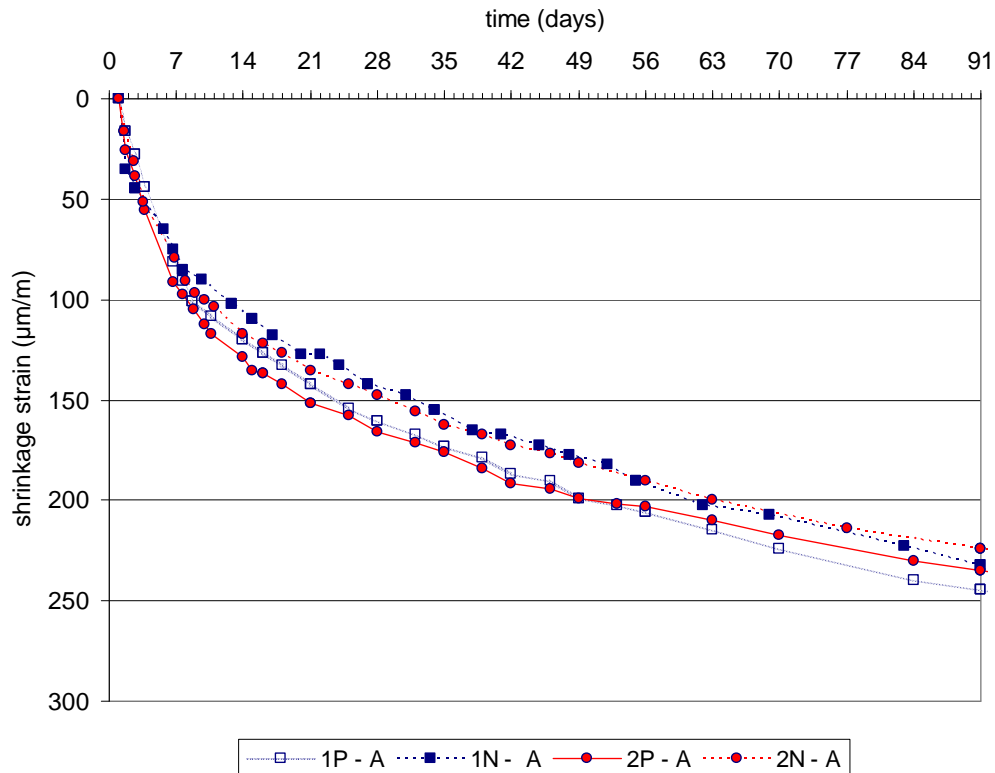


Figure 38 Sealed shrinkage, both limestone mixtures (dashed line) and fibre mixtures, wcr \approx 0.50 (blue) and 0.45

3.2.5 Autogenous shrinkage

Sealed specimens are used to determine magnitude of autogenous shrinkage. Results on weight loss of these sealed specimens during the test are used for estimation of the actual autogenous part of the measurements. Ten continuously weighed sealed specimens are used to determine the general course of weight loss, of which five are used for determination of weight loss combined with shrinkage, one per mixture type except for one traditional mixture (wcr 0.44). All 25 sealed specimens were weighed on day 1, 91 and 197 and are used to determine average weight loss.

Weight loss in time seems to be linear for the ten specimens (Figure 39). Initial mass increase is witnessed, being about 0.2 ‰ of the mass of the specimen. An explanation is not readily available, possibly ongoing hydration led to initial water uptake by the specimen, followed by drying. Total weight loss is about 1% of the initial water content. For the five specimens the occurring strain shows an approximately linear relation with the mass loss in time, the average value being 15 $\mu\text{m}/\text{m}/\text{g}$. Using all 25 sealed specimens to determine the average weight loss per day gives 0.06 g/d. The strain per day caused by weight loss is therefore 0.90 $\mu\text{m}/\text{m}/\text{d}$. This value is used to correct the sealed shrinkage for drying, obtaining an approximation for the autogenous shrinkage (Figure 40) being 120~140 $\mu\text{m}/\text{m}$ at 28 days. The development of autogenous shrinkage appears to flatten out in time. Observations from sealed shrinkage still hold (paragraph 3.2.4).

Figure 41 shows measured autogenous shrinkage strain (corrected) and elongation at break for both the traditional mixture (T) and the fibre concrete (P) with a wcr of 0.50. The strain capacity of a C28/35 concrete at 28 days is assumed to be 120 $\mu\text{m}/\text{m}$.² Strain capacity of the fibre concrete is taken lower by 10%, as was found in paragraph 3.1.2. In both cases the measured autogenous shrinkage is much higher than the elongation at break for the concrete.

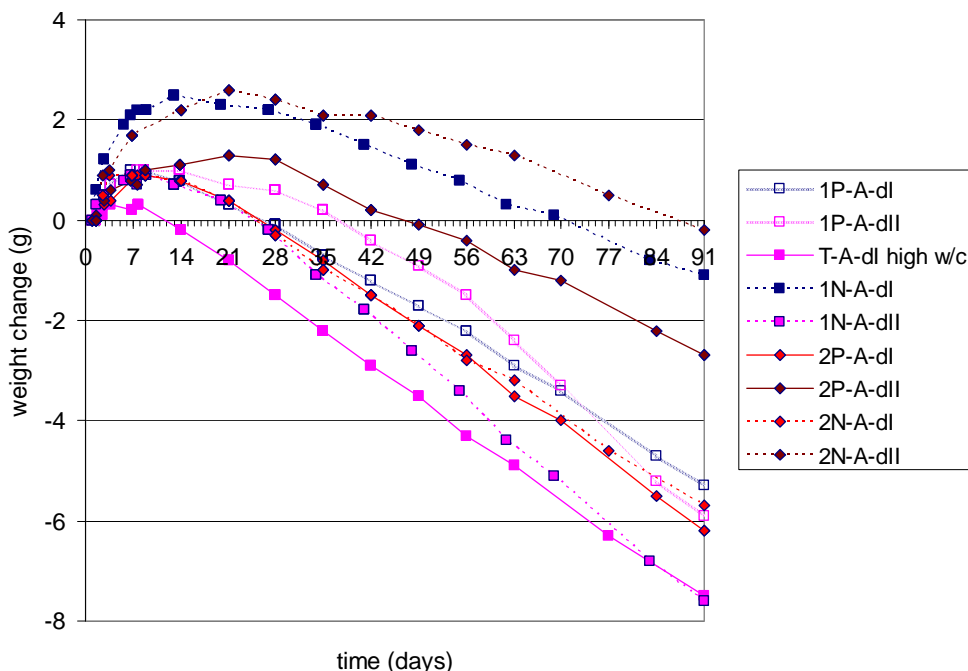


Figure 39 Weight change sealed specimens in time, where:
P = fibre mixture, N = limestone mixture, T = traditional mixture, dI, dII = specimen number

² This is based on the values from the EuroCode regarding tensile strength and modulus of elasticity for concrete. The maximum strain, or elongation at break, is found by taking the quotient of the maximum tensile stress and the modulus of elasticity.

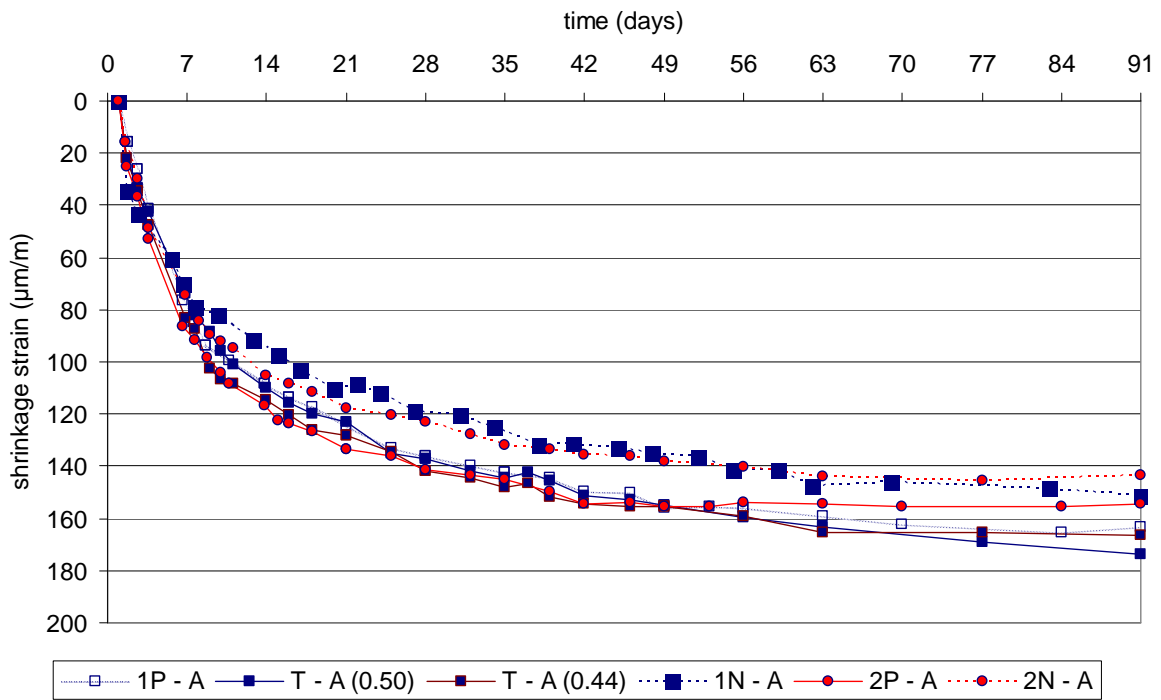


Figure 40 Estimation autogenous shrinkage by correcting sealed shrinkage for drying, where: P = fibre mixture, N = limestone mixture, T = traditional mixture

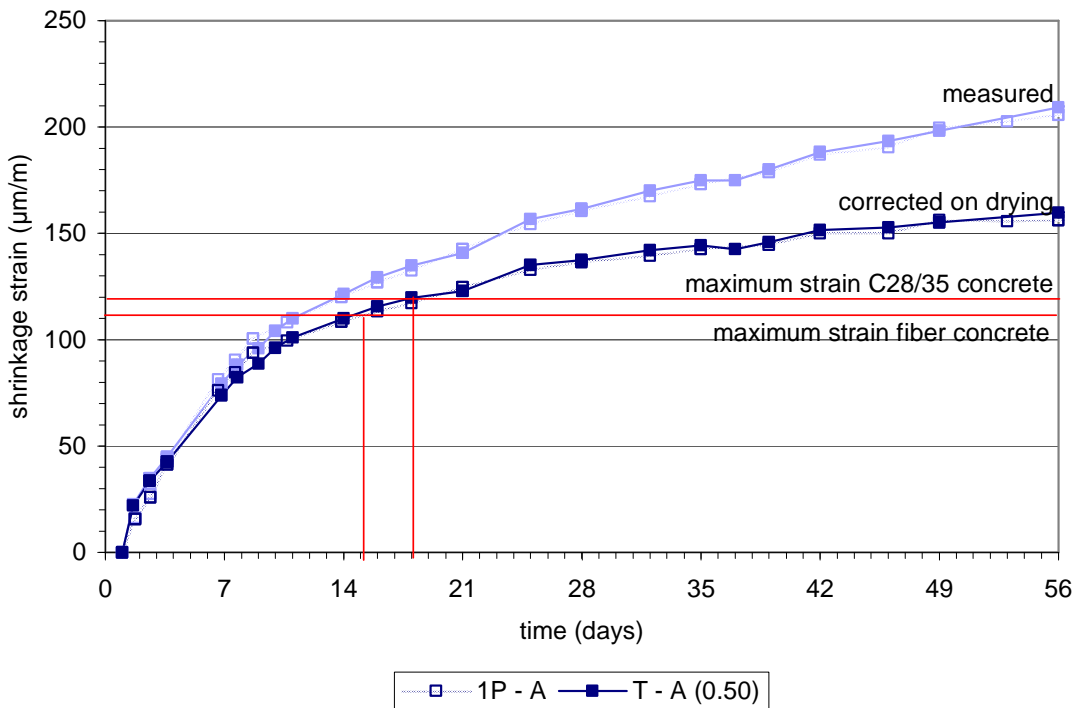


Figure 41 Autogenous shrinkage (corrected) and the elongation at break for concrete (wcr 0.50), where: P = fibre mixture, T = traditional mixture

3.2.6 Comparison with prediction models EuroCode and JSCE

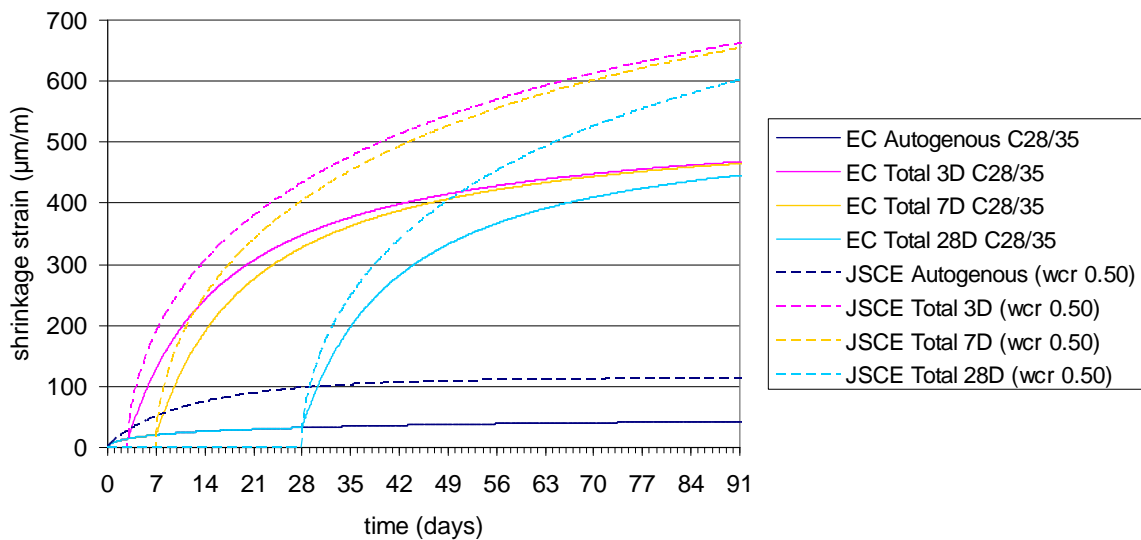


Figure 42 Prediction models from EC and JSCE, autogenous and total shrinkage

Figure 42 shows the shrinkage prediction models for both EC and JSCE, with larger strains in the JSCE prediction model. Figure 43 contains the development of autogenous shrinkage as proposed by both models for OPC concrete, together with the measured values for sealed shrinkage (measured) and the values for autogenous shrinkage (corrected on drying). A factor two between the both codes can be seen, still the measured autogenous shrinkage strain is higher than the values from both models.

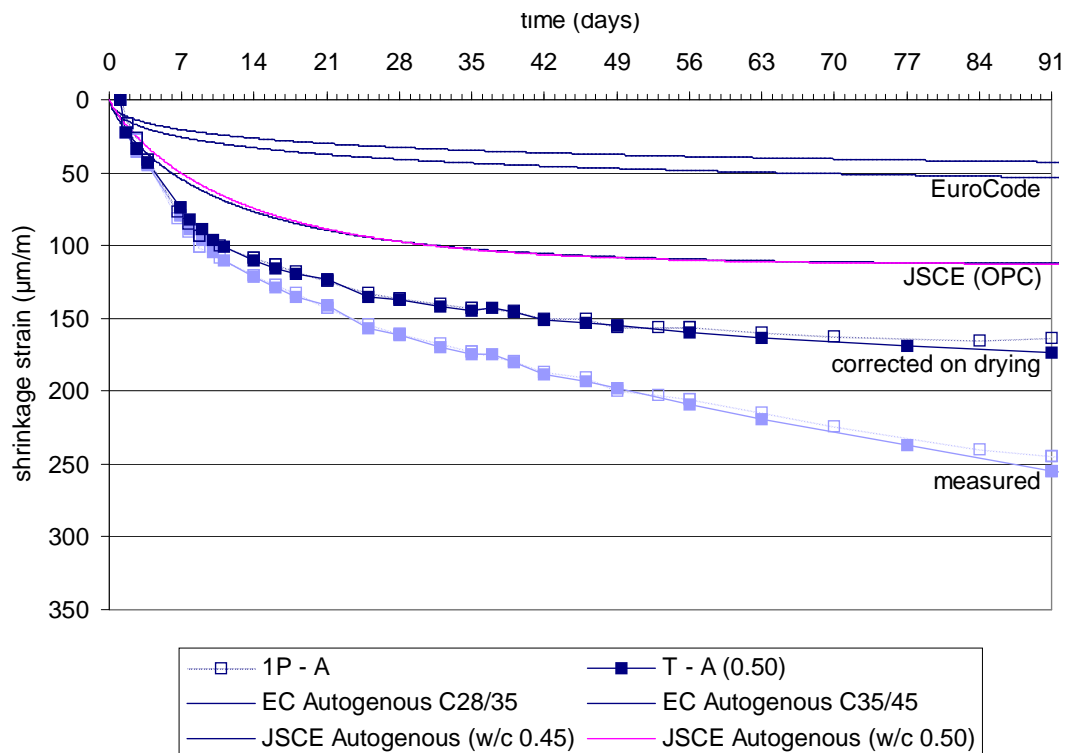


Figure 43 Autogenous shrinkage measured (corrected) and values EuroCode and JSCE

Figure 44 gives an impression of the shrinkage according to the EuroCode and the measured shrinkage. Ratio between measured total shrinkage and the calculated shrinkage according to the EuroCode model is indicated on the vertical axis of Figure 45. In time this ratio goes to a value around 1. A value of 1 means that the measured total shrinkage is equal to the values in the EuroCode. Figure 45 also shows the ratio between measured autogenous shrinkage (corrected for drying) and values according to the EuroCode. Measured autogenous shrinkage is a factor 3 to 5 larger than indicated in the EuroCode.

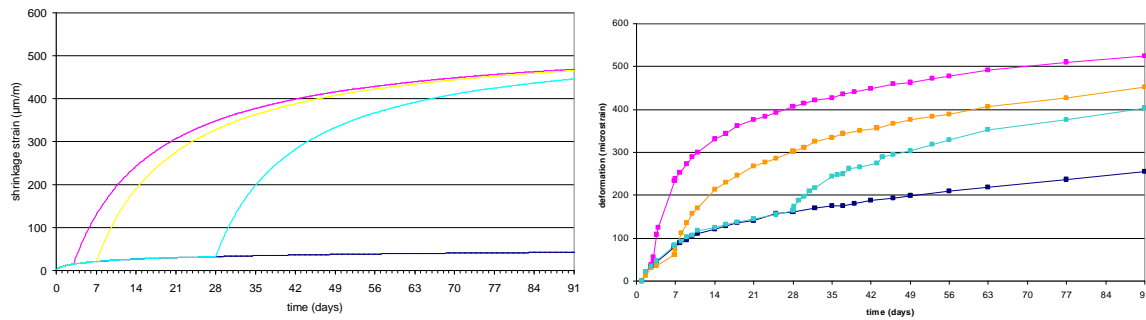


Figure 44 Impression values (total) shrinkage in EuroCode (l) and measured (r)

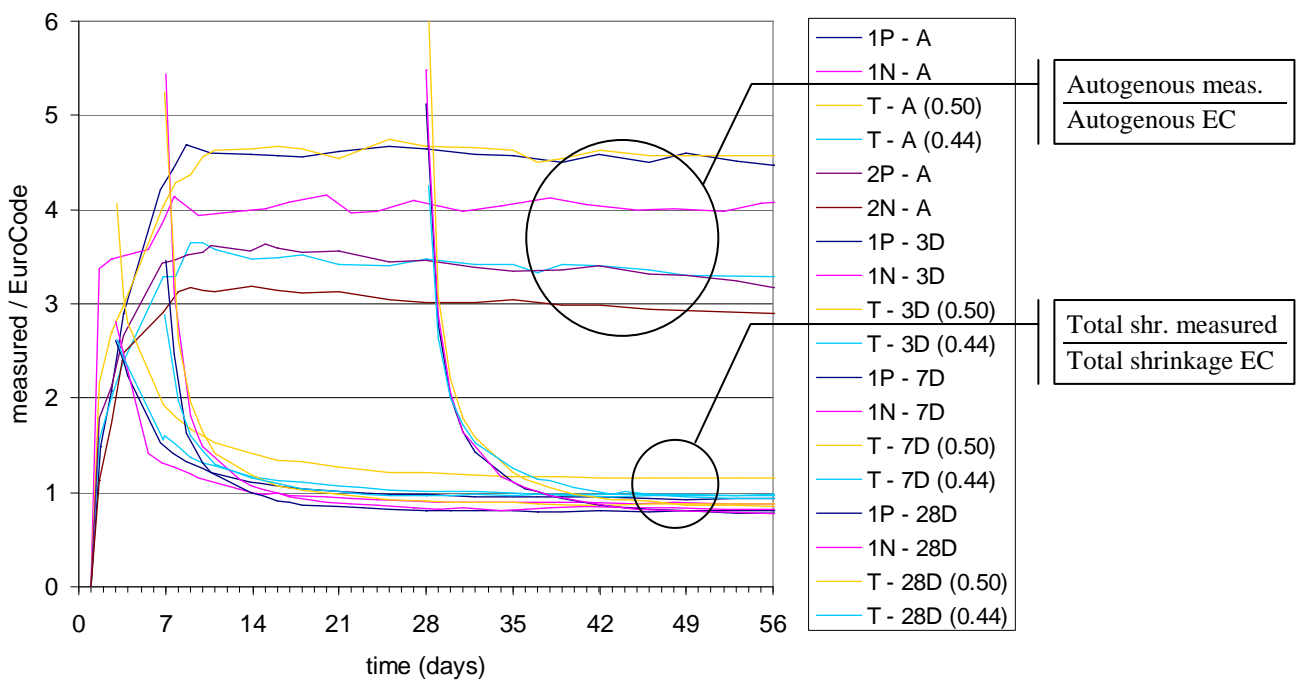


Figure 45 Ratio between measured total and autogenous shrinkage (corrected) and values EuroCode. Vertical axis: corrected values of Figure 44r (for all mixtures) divided by values of Figure 44l.

3.3 Cement paste

3.3.1 Free deformation

While tests ran for a week, results are shown until 4 days. Further measurements were on the deformations of the bottom plate, which became restrained. Results on paste of CEM I with limestone powder and one repeatability test on CEM III paste are not included, because they broke during the test. Leakage occurred due which cement paste closed the space between the bottom plate and end plate, when shrinkage occurred a compressive force was measured, that lead the device to pull the specimen apart.

Figure 46 shows measured free deformation of the pastes, zeroed at the time initial stress occurred from the self-induced stress tests (paragraph 3.3.2). Figure 47 shows the general trends that can be found from measurements on OPC and BFS cement pastes. Influence of filler material is neglected, since results are very similar and only one measurement is taken. A significant difference in shrinkage development is found between the two cement types. In case of BFS expansion occurs, which becomes neutralized by shrinkage between 2~3 days, for OPC magnitude and duration of expansion are lower. Development rate of shrinkage and magnitude are higher with BFS cement than with OPC.

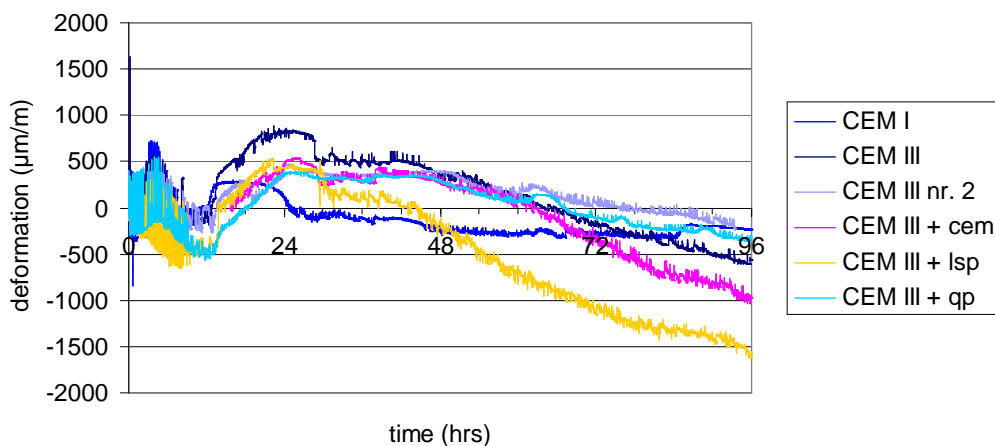


Figure 46 Free deformation measurements pastes

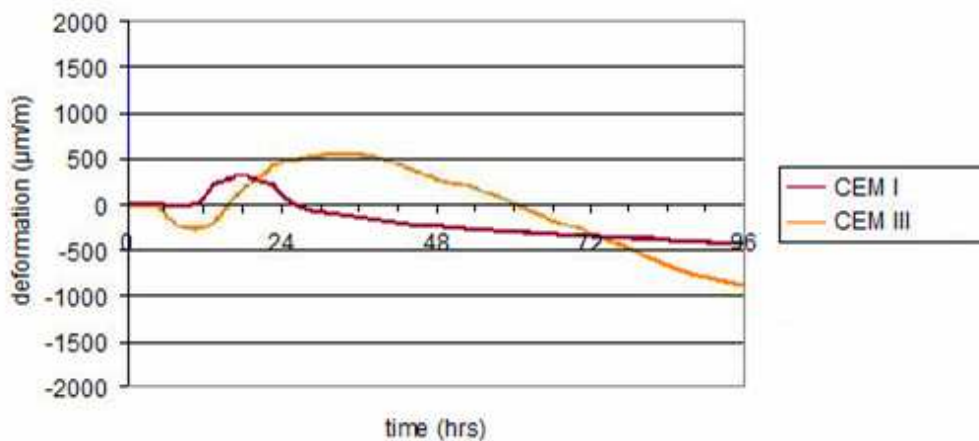


Figure 47 Global trend free deformation pastes with OPC (CEM I) and BFS (CEM III)

3.3.2 Self-induced stress

In case of CEM I with limestone powder friction occurred during the test, due which the results are less trustworthy.

Figure 48 shows measured self-induced stresses of the pastes, stress initiation determines time zero for free deformation tests. Figure 49 shows the general trends that can be found from measurements on OPC and BFS cement pastes, neglecting influence of filler material, which is approximately equal to the trends found for free deformation (paragraph 3.3.1). A significant difference in shrinkage development is found between the two materials. In case of BFS compressive stresses occur, which become neutralized between 2~3 days. Rate of stress increase is higher than with OPC. Ultimate occurring tensile stresses are higher in case of BFS.

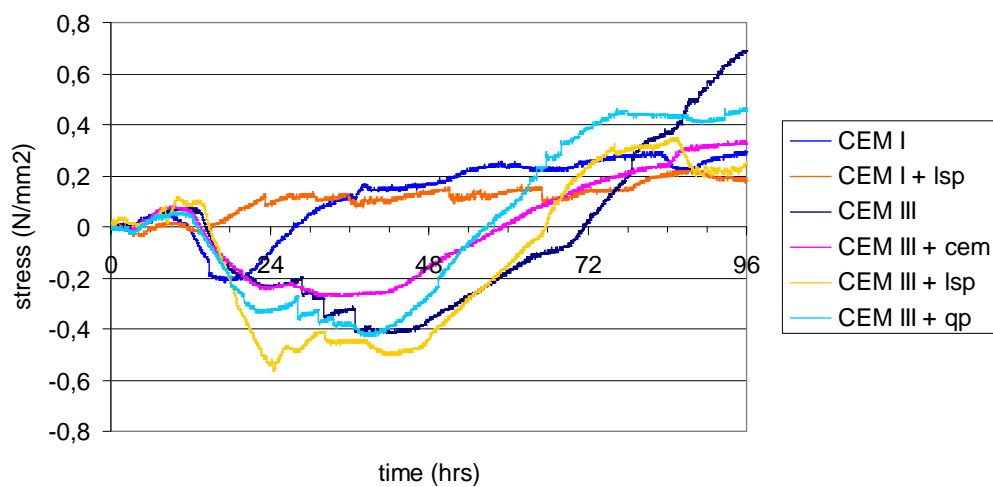


Figure 48 Self induced stress measurements pastes

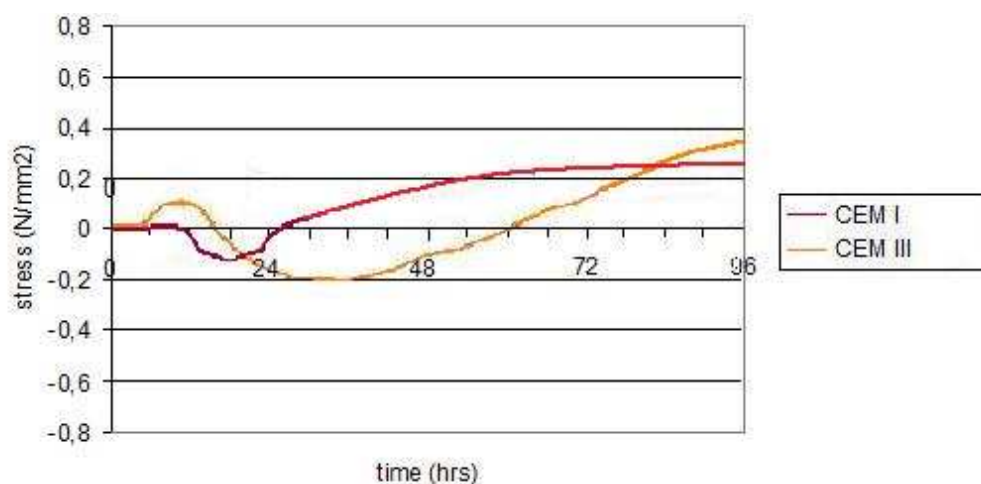


Figure 49 Global trend self induced stress pastes with OPC (CEM I) and BFS (CEM III)

3.3.3 Maximum stress at restrained and free deformation

Table 9 shows available results of maximum stress in restrained deformation and free deformation tests. Figure 50 gives an impression of the measured values in case of restrained deformation. First is the maximum occurring self-induced stress in the restrained tests. At the end of each test the specimen was deliberately cracked, giving a maximum stress at failure, the tensile strength. The tensile strength is reduced by 45~50% when specimens are restrained. Occurring stress in restrained tests is approximately 20~40% of this tensile strength.

Table 9 Comparison stress measurements during and after finishing experiments Mini-TSTM

Mini-TSTM Cement paste sample name	Restrained deformation			Free deformation	Comparison
	Stress [MPa] measured	failure	Ratio [%] $\sigma_{\text{meas}} / \sigma_{\text{fail}}$	Stress [MPa] failure	Ratio σ_{fail} [%] restrained / free def.
CEM III t	0.69	0.89	78	2.04	44
	CEM 0.33	1.84	18		
	LSP 0.58	1.80	32		
	QP 0.63	1.59	39		
CEM I t	0.30	0.74	40	1.67	45
	LSP 0.22	0.97	22		

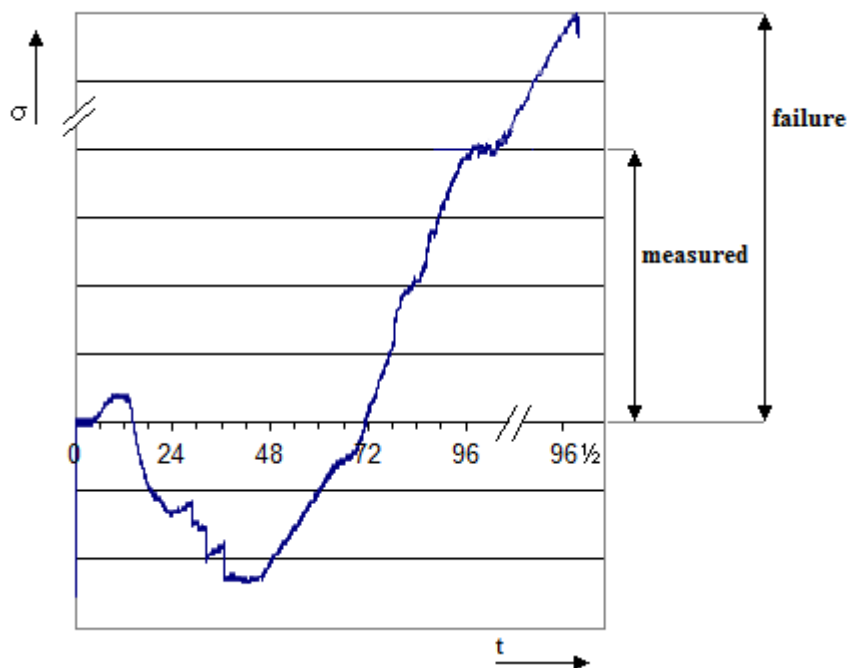


Figure 50 Impression values in table for restrained deformation tests, stress measured and failure

3.3.4 Porosity

Figure 51 shows the total porosity (dashed) and the pore size distribution of pastes at day 28. Both Portland cement pastes (CEM I) have comparable total porosity, addition of a limestone filler shows no significant influence. The total porosity is significantly lower than that of all BFS cement pastes (CEM III). Here addition of extra cement lowers the total porosity, replacement of the extra cement for a limestone filler further decreases porosity. BFS cement pastes show a more refined PSD than OPC pastes, except when a limestone powder is added. Given the ongoing hydration of BFS cement, further pore size refinement and decrease in porosity is expected for pastes containing CEM III.

Figure 52 shows densities of the materials for bulk and the skeleton. Bulk density is lower for BFS cement pastes, but skeletal densities are higher, except when limestone powder is added. In case of BFS counts that for the same volume less material is available (more porosity), but within the material there is more dense material (finer pore structure).

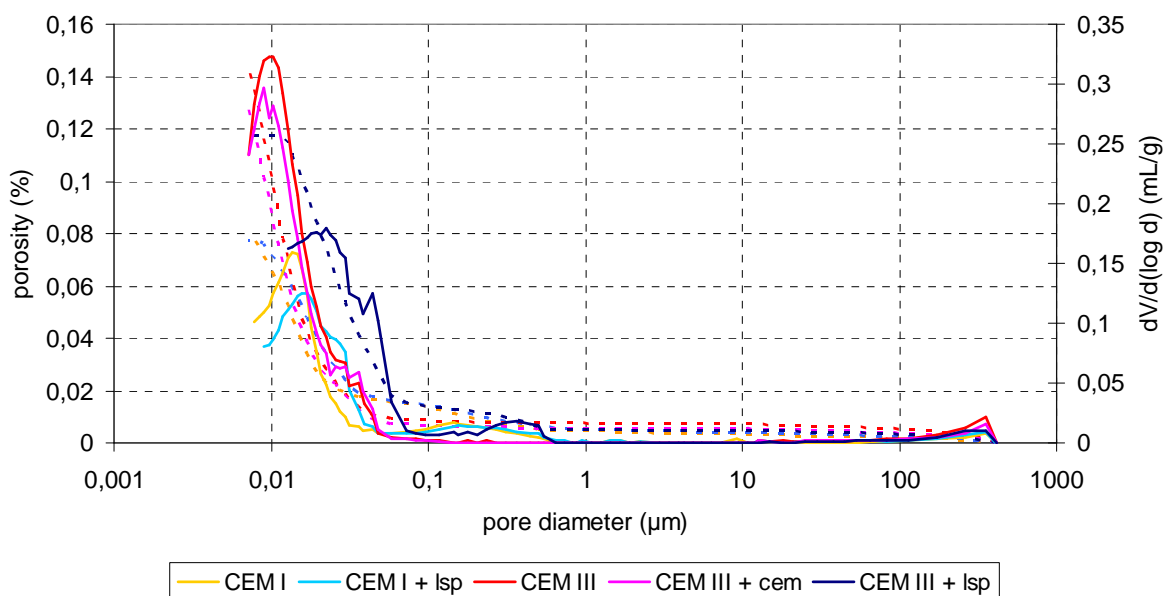


Figure 51 Cumulative pore size distribution (dashed) and differential pore size distribution pastes 28 days

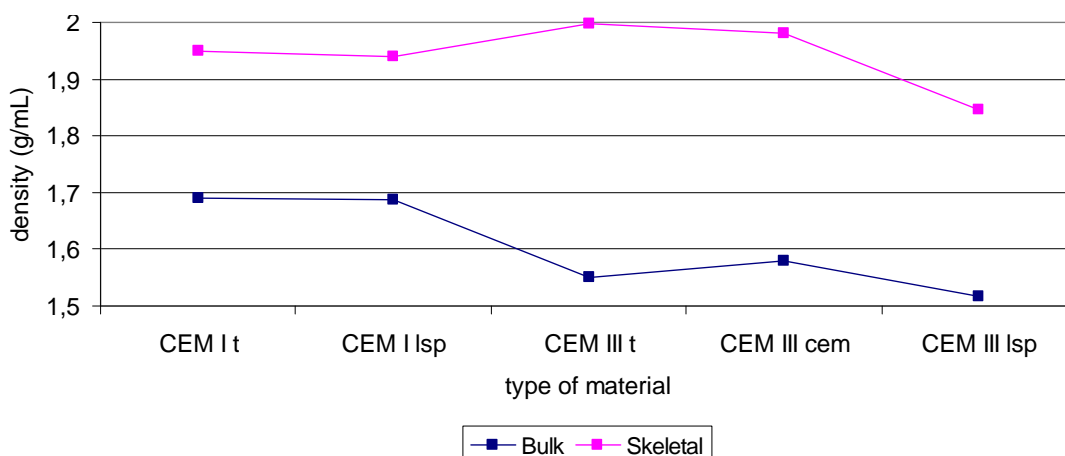


Figure 52 Bulk density and apparent (skeletal) density pastes 28 days

Chapter 4

Discussion

Together with evaluation of the results, conclusions are derived which answer the proposed research questions in the introduction. Thereby are limitations of the research acknowledged. Further included are recommendations for practice and continuing development of the Mini-TSTM, followed by advice for future research.

4.1 Discussion results

Sealed shrinkage showed an ever increasing shrinkage, at day 28 about 50% of the final sealed shrinkage was met (day 196), which can also be found in literature (Lee et al., 2006). Though autogenous shrinkage may still be ongoing, it is expected to stabilize in time. This difference is contributed to drying by moisture transport through the foil, due to the high humidity difference between the inside of the specimen and the surrounding atmosphere. When taking this into account, development of autogenous shrinkage seems more flattened out in time, as expected. In case of sealed shrinkage, influence of the fibre material seems to reduce in time, furthermore the shrinkage reduces in time for the lower water to cement ratio. Reason may be a difference in moisture transfer from the material to the environment, through the foil. Therefore no conclusions are drawn from this.

Corrected autogenous shrinkage of concrete is found to be large in all cases using BFS cement, even with a wcr of 0.50. A magnitude of 140 $\mu\text{m}/\text{m}$ is found for traditional concrete at 28 days, which is similar to results in literature (Lee et al., 2006)(van Cappellen, 2009). It should be kept in mind that measurements start from day 1 and not from initial set. From experiments on cement paste it is expected that a value for net autogenous shrinkage is determined by the measurements, but that a part does not contribute to upbuilt of tensile stresses when restrained. When the expansive processes on the first day have been taken into account, autogenous shrinkage development is comparable to results found in previous research regarding comparable concrete, but with measurements starting from moment of set (Leegwater, 2006).

The final magnitude of autogenous shrinkage at day 28 is comparable to that of the strain at break according to the norms, occurring upon full restraint of the deformation and neglecting relaxation of the material. Addition of fibres leads to a slightly higher chance on cracking than the concretes without fibres, since the deformation is similar to traditional concrete, but the maximum strain is reduced with about 10%. In a practical situation loading occurs more slowly than in the laboratory setup. Due to the possibility for relaxation when fibres are applied, the reduction in maximum strain is expected to be lower than 10% for concrete in a practical application.

The difference in wcr (0.45 to 0.50) has a negligible influence on autogenous shrinkage, but a more pronounced effect on the drying shrinkage, as expected since for both full hydration is possible and only the water content differs. Addition of a limestone aggregate reduces shrinkage by about 10%, which can be explained by the increase in modulus of elasticity of about 10%. Addition of fibres to the mixture seems to cancel out the shrinkage reducing effect of the limestone aggregate. The material may be more compressible due to higher air content, this additional air in the mixture is about 1% and can likely have caused the 10% reduction in compressive strength.

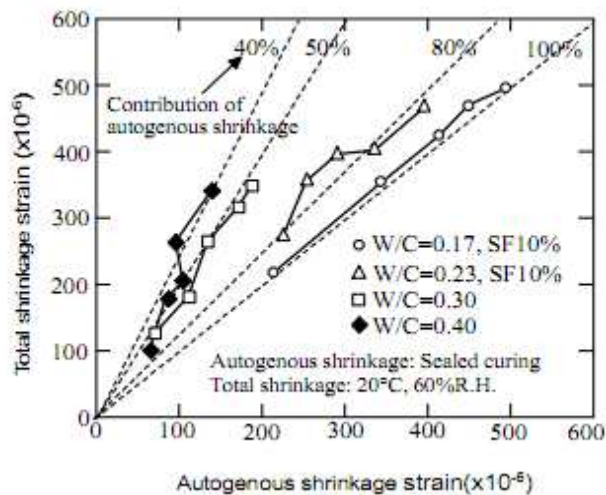


Figure 54 Ratio of autogenous shrinkage to total shrinkage (Tazawa & Miyazawa, 1997)

Total shrinkage is higher for traditional concrete than for the limestone concretes as is the shrinkage development ratio to weight loss, which may again be caused by a difference in modulus of elasticity. Addition of fibres leads to a reduction of weight loss and shrinkage ratio, possibly due to impeded moisture transfer by the effect of fibres blocking pores. Total shrinkage and weight loss is ongoing in time, meaning drying continues in time. While drying speed is lower at that point, the shrinkage development is equal to that of the sealed shrinkage, this again gives the idea sealed shrinkage is mainly caused by drying at that time, being more evenly distributed over the cross-section. Total shrinkage consists for approximately 50% of autogenous shrinkage at 28 days, slightly higher to what is expected from literature on concrete with OPC (Figure 54).

Total shrinkage relates well to the set values in prediction models used in practice, which is in case of the Netherlands contained in the EuroCode. In case of using BFS cement (CEM III/B) the found ratio of autogenous and drying shrinkage within total shrinkage does differ from the EuroCode, which is based on OPC. Measured autogenous shrinkage (corrected) is 3~5 times the value from the predicted value. Even when taking into account expansion for the first 2~3 days a factor 3.5 remains for traditional concrete (wcr 0.50).

Prediction from the codes in Japan comes closer to the measured values. For the traditional mixtures the difference is a factor 1.35 with the prediction for concrete with OPC, which can be accounted for through the factor for cement type. Furthermore the codes in Japan show a negligible influence from the difference in wcr for high water contents.

Results from experiments on cement pastes show a significant difference in shrinkage development for materials with OPC and BFS cement. A higher final shrinkage is measured when using BFS cement with a higher development rate. The first 2~3 days an expansion occurs, in case of OPC this is only during the first day and of a lower magnitude. Restrained deformation tests confirm this behaviour. Initially compressive stresses are induced which have a similar magnitude and duration, furthermore stress development and magnitude of final tensile stress is higher when BFS cement is used.

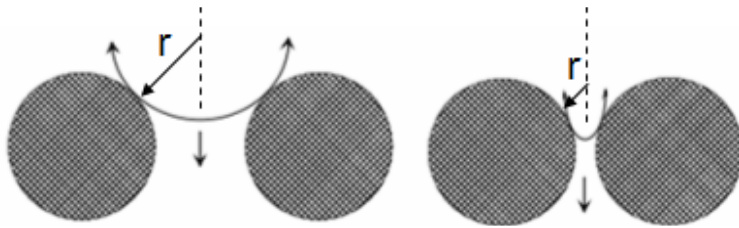


Figure 55 Smaller pore size leading to decrease radius meniscus (after Holt, 2001)

Larger shrinkage can be explained by the capillary tension approach. Porosity measurements show a more refined pore network for pastes with BFS. Smaller pore sizes give reduced radii of water menisci (Figure 55), increasing capillary tension, which enlarges shrinkage.

Restrained deformation tests on cement paste showed self-induced stresses under autogenous conditions of a magnitude approximately 20~40% of the tensile strength. Compared to freely deformed specimens, restrain causes a reduction of the tensile strength of about 45~50%, which may be explained by microcracking in the cement paste. Microcracking is then also expected in concrete, even in case of free deformation, since aggregates impose a restraint on the cement paste. This idea is confirmed by earlier research (Figure 56), where microcracking was found in unrestrained ADTM concrete specimens of a similar material (Leegwater, 2006).

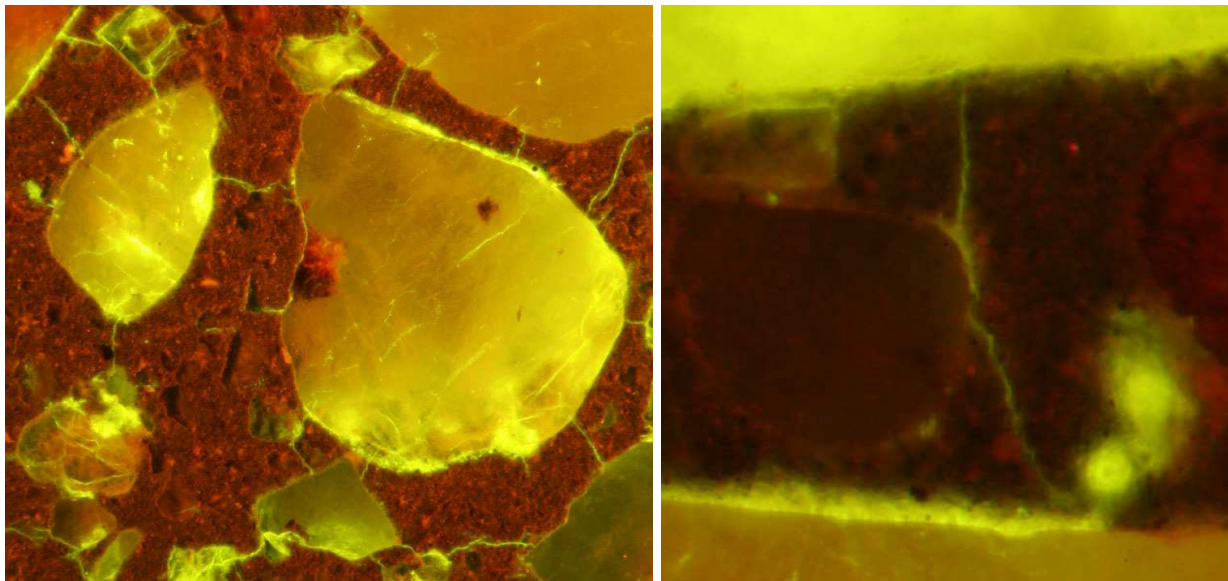


Figure 56 Microcracking ADTM specimen, CEM III/B, wcr 0.44, free deformation (Leegwater, 2006)

4.2 Limitations of Mini-TSTM

More research is needed on the Mini-TSTM, but it seems to provide a promising method for shrinkage experiments on cement paste. Due to the size of the specimens, measurements are quite sensitive to relatively small distortions, both internal and external. Measurements on the Mini-TSTM are not conducted in a climate controlled room, so that temperature and moisture content of the surrounding air changes throughout the day. After several days, results of deformation and stress tests show unexpected behaviour, which seems to have a 24 hour cycle.

Most materials used in the device have a similar thermal expansion coefficient. Metals and cement mixtures used have a maximum linear CTE of $16.5 \mu\text{m}/\text{m}\cdot^\circ\text{C}$. Maximum measured temperature difference in the laboratory is 2°C , causing a length change of 0.033% . This is of a smaller order of magnitude than the measurement itself and is therefore neglected.

The Acetal bottom plate has a linear CTE of $84.6 \mu\text{m}/\text{m}\cdot^\circ\text{C}$, with the temperature difference of 2°C this leads to a length change of 0.1692% . When the bottom plate is restrained between the two steel end plates increase in temperature of the surroundings can cause a measured expansion. The bottom plate expands and presses against the end plate. The end plate is connected to the load cell, where a compressive force is measured. In case of free deformation the boundary condition is set to zero force, so the apparatus is steered to pull on the specimen until the compressive force is released. Given that the bottom plate has a length of 72 mm , a deformation of $12.1824 \mu\text{m}$ will be measured, which has been found for instance in measurements on the specimen containing CEM I (Figure 57).

Measurements are transported through copper wires to the amplifier and measured in milli Volts. The amplified signal is transferred to the computer, after signal processing the output is plotted. Temperature and moisture content of the surrounding air induce small distortions on the measurements during the transport to the amplifier, which may be of the same order of magnitude as the measurement signal itself. In a test on a steel specimen it was found measurements cannot be read until $2\text{--}3 \mu\text{m}$, due to high noise.

Some issues occur for determining a force displacement diagram. Before a force can be measured the load cell has to set, showing a nonlinear relation of force to displacement. For unrestrained tests this may be solved by returning to zero after applying a load and continuing the measurement from there. Due to the small displacements this is a very delicate procedure.

Special care should be taken in using the LVDT attached to the tensile testing setup. In tests on steel and polymer materials, displacement was measured with both the LVDT and an external extensometer, showing the stiffness of the setup frame to be about 1 GPa . The ratio of setup deformation (by LVDT) to actual deformation (by extensometer) is dependent on the stiffness of the test material, which is unknown. Especially tests on material with higher stiffness than the setup frame may give a difference of higher orders of magnitude.

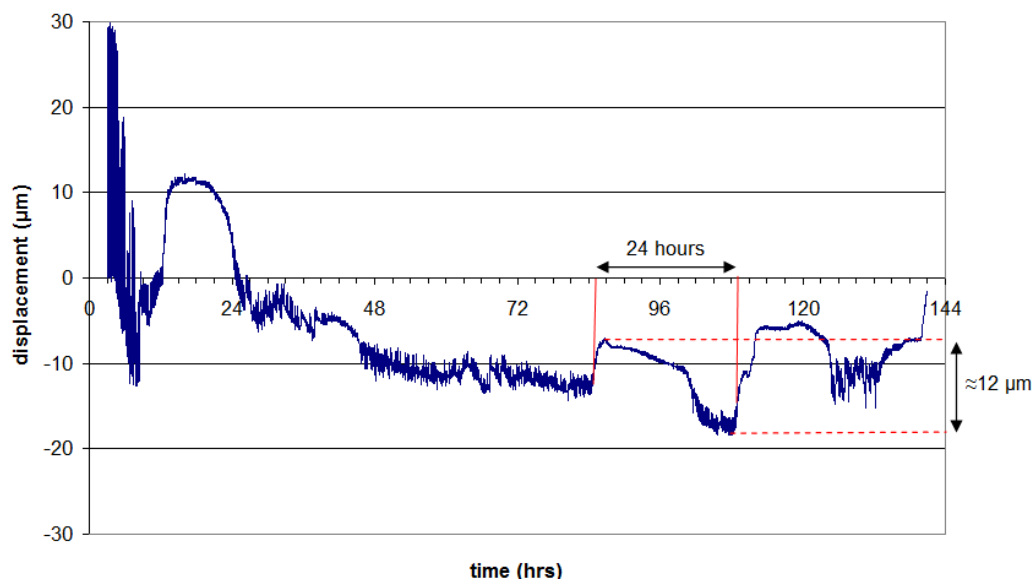


Figure 57 Displacement CEM I specimen showing temperature dependence

Current tests in the Mini-TSTM have been isothermal, at room temperature. In earlier research in Delft it was proposed to conduct tests at higher temperatures or even under adiabatic conditions, to simulate material that coincides more with building practice. Because of the size, temperature of the surroundings will be equal to temperature of the specimen. The device fits in a climate room, which can be programmed to follow a certain temperature course. Temperature development under adiabatic conditions can be determined by an experiment and inputted. However, it is important to keep in mind that the device and measurement equipment is sensitive to temperature change. Also, the device is intended to be used in stable conditions. Limitations should be well known before conducting such experiments.

4.3 Conclusions

In this thesis, autogenous deformations have been measured for concretes and cement pastes in order to determine the influence of the different constituents in the material. Two type of concretes used in practice served as a basis, gravel concrete and fire resisting concrete.

When using BFS cement and relatively high water to cement ratios of 0.45~0.50, autogenous shrinkage is quite significant for all cases examined. It contributes for about 50% of the total shrinkage and should not be neglected.

In this range of high water content the difference in water to cement ratio shows no significant effect on the autogenous shrinkage. Changing the aggregates from gravel to limestone, a stiffer material, slightly reduces autogenous shrinkage. Subsequent addition of polypropylene fibres negates the shrinkage reducing effect of the limestone aggregates.

Air content of the mixture upon addition of fibres is increased by 1%, which is taken as the main cause for the reduction in compressive strength and the increase in autogenous shrinkage, when compared to the limestone mixture without fibres. When using limestone as a coarse aggregate elongation at break becomes reduced.

Preliminary research on cement pastes revealed a clear difference in development of autogenous deformation when BFS cement is used instead of OPC. Initially expansion occurs, followed by shrinkage that develops quicker and becomes of a higher magnitude. For addition of a limestone or quartz filler material of this content no notable influence on autogenous deformation is found.

Tensile strengths are found to be reduced by 45~50% when deformations are restrained. Self-induced stress by full restraint of autogenous deformations is 20~40% of that tensile strength.

Total shrinkage from the prediction model as proposed in the EuroCode relates well to values measured on the concrete specimens. Subdivision of autogenous and drying shrinkage differs substantially, even when values are corrected and initial expansion is taken into account. Autogenous shrinkage prediction from JSCE specifications gives more satisfactory results.

Given the magnitude of autogenous shrinkage, there is an indication for cracking upon restraint and neglecting relaxation, for fire resisting concrete the chance is slightly increased.

4.4 Recommendations

4.4.1 Practice, EuroCode

Magnitude of autogenous shrinkage can not be neglected when using mixtures containing BFS cement (CEM III/B), even for a water to cement ratio of 0.45 to 0.50. Applying the EuroCode for total shrinkage gives good results, although the subdivision between autogenous and drying shrinkage is different. In case drying shrinkage is neglected, not taking into account autogenous shrinkage leads to an underestimation of the magnitude of shrinkage.

4.4.2 Development Mini-TSTM

Using the Mini-TSTM as a test setup for measuring deformation and stress development in cement pastes is a relatively new method and still under development. First results are promising, but can not be used for scientific conclusions. Performance of tests conducted with aid of the Mini-TSTM has to be investigated more extensively. Also some improvements can be made on the tensile setup and Mini-TSTM insert.

For the Mini-TSTM insert, transition between the wedge-shaped end parts and the straight sides of the mould can be more continuous and smooth. The distance between both wedge-shaped parts is smaller than the distance between both sides of the mould, which leads to stress concentrations. To make sure measured stresses occur at the prismatic part, the cross section of the prismatic part has to be governing.

Long term measurements can be conducted in a climate controlled chamber, with a constant temperature and relative humidity, to limit influences of the surrounding environment. Recommended is to amplify the measurement signal of the tensile stress setup directly on the apparatus, then transport the amplified signal to the computer. Distortions will still occur, but the measurement signal will be of higher order of magnitude than the noise signal.

The function generator during the tests with the Mini-TSTM have been set on $\Delta\text{force} = 0$ for free deformation, measuring autogenous deformation, or $\Delta\text{displacement} = 0$ for full restraint, measuring self induced stresses under autogenous conditions. In practice restraint deformation induces stresses, but the degree of restraint is not 100%. It may be possible to introduce a dynamic mode in the function generator, as is also the case for the full sized TSTM. Using results from the specimen, the function generator reduces the force with a factor depending on the degree of restraint and allows this on the specimen in the Mini-TSTM. In this way the influence of degree of restraint can be determined for material properties. The material behaviour under restraint can be used as input in a model to determine structural behaviour.

4.5 Future research

There is a difference in behaviour for BFS compared to OPC in case of autogenous shrinkage. Fundamental research may give clarity about the background of this difference.

Measurements on cement pastes indicate a reduction on tensile strength when deformations are restrained. Within the concrete material restraint is expected, for instance by the aggregates. More research may give an insight on tensile strength reduction by autogenous deformations.

Influence can be determined on internal humidity change by moisture transport through foils of sealed specimens, possibly leading to a change in method of execution for future research under autogenous conditions.

In case of concrete with BFS cement, care should be taken with drawing conclusions when measurements start after one day, valuable information may be lost. In order to understand the influence of autogenous shrinkage on stress and crack formation in practice, more research can be conducted for mixtures containing BFS cement (CEM III/B) and water to cement ratios of 0.40 to 0.50. Full size ADTM / TSTM tests for concrete can be used to determine magnitude and development of autogenous deformations, self induced stresses upon restricted deformations and the development of the general properties of the concrete mixture in time.

A practical case can be used to relate laboratory outcomes to measurements in practice. Strain gauges can be embedded in the concrete during or just after casting. Another possibility is to insert a strain gauge into the hole of a drilled core, after demoulding. Shrinkage development can be compared to development of general properties.

References

- ACI (2002), Committee 544 "Fiber Reinforced Concrete", State-of-the-Art Report on Fiber Reinforced Concrete, Reapproved.
- Acker, P. (1988), Comportement mécanique du béton: apports de l'approche physico-chimique, Rapport de Recherche LPC, No 152.
- Bangham, D.H. (1937), The Gibbs Adsorption Equation and Absorption on Solids, London, Gurney and Jackson.
- Barcelo, L. (2002), "Chemical shrinkage", Early age cracking in cementitious systems, ed. A. Bentur, RILEM TC 181-EAS Committee, RILEM, Cachan, pp. 22-28.
- Baroghel-Bouny, V. (1996), "Texture and Moisture Properties of Ordinary and High Performance Cementitious Materials", Proceedings of Seminaire RILEM 'Benton: du Matériau à la Structure', Arles, France.
- Bažant, Z.P., Wittmann, F.H. (1982), Creep and Shrinkage in Concrete Structures, John Wiley & Sons, New York, pp. 363.
- Beek, A. van (1995), Determination of strength of hardening concrete - Universal Concrete Curing CONTROL system (in Dutch), Master thesis, Delft University of Technology, pp. 97.
- Bentz, D.P. (2007), "Internal Curing of High Performance Blended Cement Mortars", ACI Materials Journal, 104 (4), pp. 408-414.
- Bentz, D.P. (2009), "Early Age Cracking Review: Mechanisms, Material Properties, and Mitigation Strategies", Report prepared for Cementitious Barriers Partnership, CBP-TR-2009-002-C3.
- Bentz, D.P., Garboczi E.J. & Quenard, D.A. (1998), "Modelling drying shrinkage in reconstructed porous materials: application to porous Vycor glass", Modelling Simul Mater Sci Eng 6, pp. 211-236.
- Bentz, D.P., Weiss, W.J. (2011), NIST Report "Internal Curing: A 2010 State-of-the Art Review" NISTIR 7765, ed. D.P. Bentz & W.J. Weiss.
- Bjøntegaard, Ø. (1999), Thermal dilation and autogenous deformation as driving forces to self-induced stresses in high performance concrete, Ph.D. thesis, NTNU Division of Structural Engineering, Trondheim, Norway.
- Bossche, B.P. van den (2008), Brandwerend beton (in Dutch), Cement 2008 4, pp. 42-46.
- Breugel, K. van (1991), Simulation of hydration and formation of structure in hardening cement-based materials, Ph.D. thesis, Delft University of Technology, Delft, The Netherlands.
- Cappellen, J. van (2009), Autogenous and drying shrinkage, M.Sc. thesis, Delft University of Technology, Delft, The Netherlands.
- Chartschenko, I., Stark, J. (1995), "Über die Bedeutung der Nachbehandlung bei der Erhärtung von Quellzementen", Wiss. Z. Hochsch. Archit. Bauwes. - Weimar 41: 167-173.

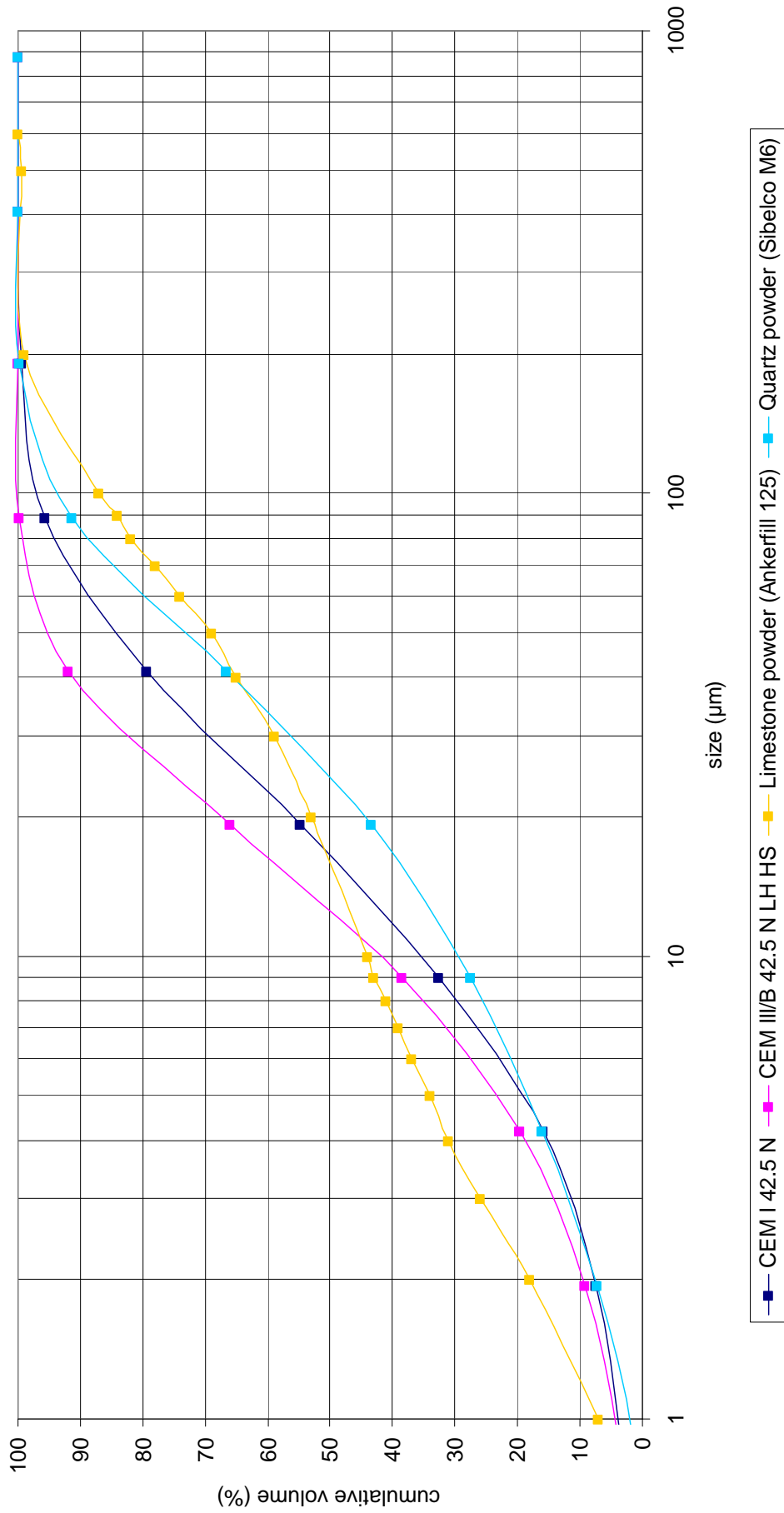
- Chen, W. (2006), Hydration of Slag Cement - Theory, Modeling and Application, Ph.D. thesis, University of Twente, Enschede, The Netherlands.
- Eurocode 2-1 (2005), Design of Concrete Structures: General Rules and Rules for Buildings.
- Feldman, R.F. (1983), "Significance of porosity measurements on blended cement performance", Proc. of the CANMET/ACI 1st int. conf. on the use of FA, SF, slag and other mineral by-products in Concrete, Montebello, Quebec, Canada, Vol. 1, SP-79, pp. 415-433.
- Geiker, M., Knudsen, T. (1982), "Chemical shrinkage of Portland cement pastes", Cement and Concrete Research 12(5) pp. 603-610.
- Hanehara, S., Hirao, H. and Uchikawa H. (1998), "Relationships between autogenous shrinkage, and the microstructure and humidity changes at inner part of hardened cement paste at early age", Proc. of the Int. Workshop on Autogenous Shrinkage of Concrete, Autoshrink'98, JCI, Hiroshima, Japan.
- Hansen, W. (1987), "Constitutive Model for Predicting Ultimate Drying Shrinkage of Concrete", Journal of the American Ceramic Society 70 (5) pp. 329-332.
- Holt, E.E. (2001), Early age autogenous shrinkage of concrete, VTT Building and Transport, Technical Research Centre of Finland, Espoo, Finland.
- Iragashi, S., Bentur, A. and Kovler, K. (1999), "Stresses and Creep Relaxation Induced in Restrained Autogenous Shrinkage of High-Strength Pastes and Concrete", Advances in Cement Research 11 (4) pp. 169-177.
- JCI (1998), Technical committee on autogenous shrinkage of concrete, Autoshrink'98, Proc.Int. Workshop, ed. E. Tazawa, Hiroshima, Japan.
- Jensen, O.M. (1993), Autogenous deformation and RH-change – self-desiccation and self-desiccation shrinkage (in Danish), Ph.D. thesis, TR 284/93, Building Materials Laboratory, Technical University of Denmark, Lyngby.
- Jensen, O.M., Hansen, P.F. (1996), "Autogenous deformation and change of the relative humidity in silica fume-modified cement paste", ACI Materials Journal 93 (6) 539-543.
- JSCE (1996, 2002), "Standard specification for design and construction of concrete structures, part I [Construction]" (in Japanese), JSCE, Tokyo, Japan.
- Koenders, E.A.B. (1997), Simulation of volume changes in hardening cement-based materials, Delft University of Technology, Ph.D. thesis, Delft, The Netherlands.
- Kondo, R., Ohsawa, S. (1968), "Studies on a method to determine the amount of granulated blastfurnace slag and the rate of hydration of slag in cement", Proc. 5th ICCS, Vol.4, Cement Association of Japan, Tokyo, Japan, pp. 255-269.
- Lange, D.A. (2002), "Overview of Driving Forces", Report of TC 181-EAS, ed. A. Bentur, Early age cracking in Cementitious systems, RILEM, France (2002), pp. 19-21.
- Le Chatelier, H. (1900), "Sur les changements de volume qui accompagnent le durcissement des ciments", Bullet. de la société d'encouragement pour l'industrie nationale 5 (5) pp. 54-57.
- Lee, K.M., Lee H.K., Lee, S.H., Kim, G.Y. (2006), "Autogenous shrinkage of concrete containing gbfs", Cement and Concrete Research 36 (7), pp. 1279-1285.

- Leegwater, G.A. (2006), Autogenous deformation in cement paste and the effects on concrete behavior, M.Sc. thesis, Delft University of Technology, Delft, The Netherlands.
- Locher, F.W., et al. (1976), "Erstarren von Zement", *Zement Kalk Gips* 29 (10) pp.435-442.
- Lokhorst, S.J. (1999), Deformational behaviour of concrete influenced by hydration related changes of the microstructure, Research Report, Delft University of Technology, Delft, The Netherlands.
- Lura, P. (2003), Autogenous deformation and internal curing of concrete, Ph.D. thesis, Delft University of Technology, Delft, The Netherlands.
- Lura, P., Jensen, O.M. (2005), "Volumetric Measurement in Water Bath - An Inappropriate Method to Measure Autogenous Strain of Cement Paste", PCA R&D Serial No. 2925, Portland Cement Association, Skokie, IL, U.S.
- Mehta, P.K., Monteiro, J.M. (1993), *Concrete structure, Properties and Materials*, 2nd Edition, Prentice Hall, Inc., 1993, pp. 548.
- Mindess, S., Young, J.F. (1981), *Concrete*, Prentice-Hall, Inc., Englewood Cliffs, NJ, U.S.
- Miyazawa, S., Tazawa, E. (2005), "Prediction model for autogenous shrinkage of concrete with different types of cement", Report TVBM-3126, ed. B. Persson, D. Bentz and L.-O. Nilsson, Proc. Of the 4th Int. Research Seminar, Gaithersburg, Maryland, USA.
- Neville, A.M. (1995), *Properties of concrete*, John Wiley & Sons, New York.
- Pietersen, H.S. (1993), Reactivity of fly ash and slag in cement, Ph.D. thesis, Delft University of Technology, Delft, The Netherlands.
- Powers, T.C. (1935), "Absorption of water by Portland cement paste during the hardening process", *Industrial and Engineering Chemistry* 27 (7) pp. 790-794.
- Powers, T.C. (1965), "Mechanisms of shrinkage and reversible creep of hardening cement paste", in Proc. Int. Symp. Structure of Concrete and its behaviour under load, Cem. & Concr. Ass., London, pp. 319-344.
- Powers, T.C., Brownyard, T.L. (1948), "Studies of the physical properties of hardened Portland cement paste" (9 parts), *J Amer Concr Inst* 43 (Oct. 1946 to April 1947), Bulletin 22, Research Laboratories of the Portland Cement Association, Chicago.
- Puertas, F., Santos, H., Palacios, M. and Martínez-Ramírez, S. (2005), "Polycarboxylate superplasticiser admixtures: effect on hydration, microstructure and rheological behaviour in cement pastes", *Advances in Cement Research* 17 (2) pp. 77-89.
- Radocea, A. (1992), A Study on the Mechanisms of Plastic Shrinkage of Cement-Based Materials, Ph.D. thesis, CTH Göteborg, Sweden, pp. 125.
- RILEM (1982) General Report, Session I: Mechanical Properties International Conference on Concrete at Early Ages. Volume II, Paris.
- RILEM (2002), Technical Committee "Early Age Cracking in Cementitious Systems" TC 181-EAS, ed. A. Bentur, Early age cracking in cementitious systems, Cachan, pp. 388.
- ROBK (2006) (in Dutch), Afdeling Civiele Techniek, Bouwdienst Rijkswaterstaat.
- Sakata, K., Shimomura, T. (2004), "Recent Progress in Research on and Code Evaluation of Concrete Creep and Shrinkage in Japan", *Journal of Adv. Concr. Techn.* 2 (2) pp. 133-140.

- Sato, K., Konish, E. and Fukaya, K. (1986), "Hydration of blastfurnace slag particle", Proc. 8th ICC, Vol.4, Rio de Janeiro, Brazil, pp. 98-103.
- Schäfer, E. (2004), Einfluss der Reaktionen verschiedener Zemenbestandteile auf den Alkali-haushalt der Porenlösung des Zementsteins, Ph.D. thesis, Clausthal University of Technology, Clausthal-Zellerfeld, Germany.
- Soroka, I. (1979), Portland cement paste and concrete, Macmillan Press, London.
- Tanaka, H., Totani, Y. (1983), "Structure of hydrated glassy blastfurnace slag in concrete", in V.M. Malhotra (ed.), International conference on the use of FA, SF, slag, and other mineral by-products in concrete, Vol.II, ACI, Montebello, Quebec, Canada, pp. 963-977.
- Taylor, H.F.W. (1997), Cement chemistry, Thomas Telford Publishing, London.
- Tazawa, E. (1999), Autogenous shrinkage of concrete, E & FN Spon, London.
- Tazawa, E., Miyazawa, S. (1995), "Influence of cement and admixture on autogenous shrinkage of cement paste", Cem Concr Res 25 (2) pp. 281-287.
- Tazawa, E., Miyazawa, S. (1997), "Influence of cement composition on autogenous shrinkage of concrete", Proc. 10th International Congress on the Chemistry of Cement.
- Wittmann, F.H. (1977), "Grundlagen eines Modells zur Beschreibung Charakteristischer Eigenschaften des Betons", Deutscher Ausschuss für Stahlbeton 290 (197) pp. 42-101.
- Wittmann, F.H. (1992), "On the interaction of gel particles in hydrating Portland cement", Hydration and Setting of Cements, ed. A. Nonat, J.C. Mutin, RILEM, E&FN Spon, London.
- Wolter, A., Frischat, G.H. & Olbrich, E. (2003), "Investigation of granulated blast furnace slag (gbfs) reactivity by SNMS", in G. Grieve, G. Owens (ed.), Proc. 11th ICC, Vol.4, Cement & Concrete Institute, Durban, South Africa, pp. 1866-1877.

Appendices

Appendix A Particle size distribution materials pastes



Appendix B Total shrinkage concrete until 196 days

